

1 Dear editor,

2 I am pleased to send you the revised version of my paper on “Diagenetic evolution of fault
3 zones in Urgonian microporous carbonates, impact on reservoir properties (Provence – SE
4 France) with highlighted corrections.

5 You will see that most of the corrections have been respected as requested.

6 You will find below, the comments to all remarks. In addition, I made a table to survey the
7 reviewer comments with the following colour code

8 - Corrections validated are in **green**

10 - Corrections in **red** have been considered un-useful or inappropriate

11 Best regards,

12 Irène Aubert

N° line	validat.	not app.	Reviewer's remarks
18	ok		Perhaps "carbonate staining" or "staining technique" would sound better than "red
27	ok		Here please correct to the plural form "depend" instead of the singular "depends".
50	ok		Check if this structure suits better to the sentence "faulting and diagenetic
57	ok		Perhaps here "in" sounds better than "on" since you are describing fault zones
70	ok		Maybe here I would erase "the" before "Late-Cretaceous times".
70	ok		Here is better to cancel the hyphen between "Late-Cretaceous", to keep the same
71	ok		I would erase the highlighted "platform" which sounds like a repetition of what is
72	ok		Please erase "plate" after "Iberia", otherwise you will have a repetition.
85	ok		Please correct "swith" with the word "with".
88	ok		I saw you used different styles describing the trend of faults and structures. In this
89	ok		Consider changing "composed" with "composed of" or "comprising".
91	ok		Keep a space between the length and the measurement unit as follows "50 mlong
91		x	Here maybe better than "extension" you can use "outcrop".
93	ok		Same comment as in Line 88.
100	ok		Please correct "bear" with "bears".
101	ok		Same comment as in Line 88.
102	ok		Please add a space between "whichreactivated" to "which reactivated".
103	ok		Please add a space between "ledto" to "let to".
112	ok		Please add a full stop at the end of this sentence.
119-120	ok		would turn "stereographic projections" to the singular form, because in

120	ok	Please pluralise "photomicrograph" to "photomicrographs".
120	ok	Please erase one of the parenthesis at the end of the sentence.
129	ok	Here I would erase "in" after "cross-cut".
136	ok	Please erase the space after the first parenthesis
140	ok	Please correct the term with "strike-slip".
156	ok	Typically Alizarin in studies related to diagenesis and geochemistry is reported
158	ok	Here maybe is better to use the plural form "generations" instead the singular
162	ok	Decide if you want to write the number of samples in extended form or as
168	ok	Is necessary to put "Bulk" in capitals?
174	ok	Please erase "respectively".
182	ok	Please add a space between "measuredon".
184	ok	Add ":" after "mean" as you did previously in the same sentence.
188	ok	Please add a space between "than7%".
195	ok	Is necessary to put "Red" in capitals?
201	ok	Please correct "identified" with "identify".
209	ok	Here I would erase "of".
211	ok	Here I would erase "of".
215	ok	Please add "are" before "made of".
215	ok	If you are referring to calcite than you should correct to the third person form
228	ok	with maximum size of" sounds better than "sized of maximum".
229	ok	Please add "presence" after "show the".
242	ok	Here are you referring to the "FR1" matrix? If so, please correct accordingly.
243	ok	Maybe here use the plural form of "zonation" "zonations".
245	ok	Please substitute "and" with "while".
253	ok	Please add a space between "layersfrom".
256	ok	Here I believe it is preferable to use the present simple form "appears" instead of
258	ok	Please correct to the third person form "increases" instead of "increase".
268-269	ok	Please erase "transect" because there is a repetition and pluralise
277	ok	In the first line please correct the symbols you used for the delta notation, the
281	ok	Please change "deplets" with "are more depleted".

285	ok		Please correct "fluctuates" with "fluctuate".
287	ok		Please correct "ranges" with "range".
289	ok		Please correct "ranges" with "range"
291-292	ok		When you describe the isotopic interval put always as first value the most
293	ok		Please erase "respectively".
300	ok		You should add a semicolon or a full stop at the end of this sentence.
307	ok		Please erase "to".
308	ok		Please put "C2" before "cement".
311	ok		Please change "after" with "is subsequent to".
315	ok		Please add a space between ",cementation".
332	ok		Please correct to the third person form "does" instead of "do": the subject of the
333	ok		The same comment as in lines 291-292, put first the most negative value you
361	ok		At this point may sound better to write like this "deformation band development".
365	ok		Please pluralise "rocks" since you write "were likely characterised".
366	ok		Here I think "petrophysical" would suit better what you are explaining rather than
373	ok		Perhaps here this would be better and simpler "This could explain".
379		x	At this point "carbonates" may be omitted because after you write "grainstones",
391	ok		Please erase one of the full stops at the end of the sentence. There are two full
407	ok		Here maybe I would change "C3" with "it" to avoid repetition with the opening of
408	ok		Please add a space between ".The".
409	ok		Please correct "fluid" with "fluids".
429	ok		Please correct "Apennines" with "Apennine".
429	ok		Please correct "strike" with "strike-slip".
438	ok		Please add a hyphen between "short-lived".
446	ok		Please add a hyphen between "fault-related".
467	ok		Please change "leading" with "led".
467	ok		Please add a space between "Fig. 9,B7".
480	ok		See if this suggestion suits you "transects 2 and 3" instead of "transect 2 and
498	ok		Here I would erase "the" if you feel this could be an option.
498	ok		Wider better than "larger".

499	ok	Please correct "others" with "other".
499	ok	Keep a space between the length and the measurement unit "30 m and 40 m".
500	ok	Please correct "triggerred" with "triggered".
513	ok	Please correct "what" with "that".
527	ok	Please invert the order of the two words "comes mainly" to "mainly comes".
546	ok	Add a space between "8(".
547	ok	Maybe you should capitalise also "porosity".
547	ok	Decide if you want to put in capitals also "zone", but do the same both for the
573	ok	would put the comma before "and".
582	ok	Please correct to the singular form "zone".
586	ok	Please add "in" before "the damage zone".
comments on figures and captions		
table 1	ok	in the "Fault core thickness" column in the last raw at the bottom please add a
figure 5 cap.	ok	In the second sentence please correct "micritszed" to "micritised".

14 **Diagenetic evolution of fault zones in Urgonian microporous**
15 **carbonates, impact on reservoir properties (Provence – SE France).**

16

17 *Irène Aubert ^a, Philippe Léonide ^a, Juliette Lamarche ^a, Roland Salardon ^a*

18

19 *^a Aix-Marseille Université, CNRS, IRD, Cerege, Um 34, 3 Place Victor Hugo (Case 67), 13331*
20 *Marseille Cedex 03, France*

21

22

23 Microporous carbonate rocks form important reservoirs with permeability variability depending
24 on sedimentary, structural and diagenetic factors. Carbonates are very sensitive to fluid-rock
25 interactions that lead to secondary diagenetic processes like cementation and dissolution
26 capable of modifying the reservoir properties. Focusing on fault-related diagenesis, the aim of
27 this study is to identify impact of the fault zone on reservoir quality. This contribution focuses
28 on two fault zones east to La Fare Anticline (SE France) cross-cutting Urgonian microporous
29 carbonates. 122 collected samples along four transects orthogonal to fault strike were analysed.
30 Porosity values have been measured on 92 dry plugs. Diagenetic elements were determined
31 through the observation of 92 thin sections using polarized light microscopy,
32 cathodoluminescence, **carbonate staining**, SEM and stable isotopic measurements ($\delta^{13}\text{C}$ and
33 $\delta^{18}\text{O}$). Eight different calcite cementation stages and two micrite micro-fabrics were identified.
34 As a main result, this study highlights that the two fault zones acted as drains canalizing low-
35 temperature fluids at their onset, and induced calcite cementation which strongly altered and
36 modified the local reservoir properties.

37 **1. INTRODUCTION**

38 Microporous carbonates form important reservoirs (Deville de Periere et al., 2017; Lambert et
39 al., 2006; Sallier, 2005; Volery et al., 2009), with porosity values up to 35% (Deville de Periere
40 et al., 2011). Due to their heterogeneous properties which **depend** on sedimentary, structural
41 and diagenetic factors, microporous carbonates may determine a high variability of reservoir
42 permeability (Bruna et al., 2015; Deville de Periere et al., 2011, 2017; Eltom et al., 2018; Florida
43 et al., 2009; Hollis et al., 2010). Moreover, fault zones in carbonates play an important role on
44 reservoir properties (Agosta et al., 2010, 2012; Caine et al., 1996; Delle Piane et al., 2016;
45 Ferraro et al., 2019; Knipe, 1993; Laubach et al., 2010; Rossetti et al., 2011; Sinisi et al., 2016;
46 Solum et al., 2010; Solum and Huisman, 2016; Tondi, 2007; Wu et al., 2019). Fault zones are
47 complex structures composed of damage zones and the fault core encompassed by the host rock
48 (Caine et al., 1996; Chester and Logan, 1986, 1987; Hammond and Evans, 2003). Faults can
49 act as barriers (Agosta et al., 2010; Tondi, 2007), drains (Agosta et al., 2007, 2008, 2012; Delle
50 Piane et al., 2016; Evans et al., 1997; Molli et al., 2010; Reches and Dewers, 2005; Sinisi et al.,
51 2016; Solum and Huisman, 2016), or mixed hydraulic behaviour zones (Matonti et al., 2012)
52 depending on their architecture and diagenetic evolution. Because of their hydraulic properties,
53 fault zones influence the fluid flows in the upper part of Earth's crust (Bense et al., 2013; Evans
54 et al., 1997; Knipe, 1993; Sibson, 1994; Zhang et al., 2008), and are capable of increasing the
55 fluid-rock interactions. Carbonates are very sensitive to these interactions, which lead to
56 diagenetic secondary processes like cementation and dissolution (Deville de Periere et al., 2017;

57 Fournier and Borgomano, 2009; Lambert et al., 2006). Fault-related diagenesis locally modifies
58 the initial rock properties (mineralogy and porosity), and therefore the reservoir properties
59 (Hodson et al., 2016; Knipe, 1993; Knipe et al., 1998; Laubach et al., 2010; Woodcock et al.,
60 2007). In case of a polyphasic fault zone, repeating fluid pathways-barriers behaviour in times
61 leads to very complex diagenetic modifications. The initial vertical and lateral
62 compartmentalization of microporous limestones is, therefore, accentuated by fault-related
63 diagenesis. Hence, understanding **faulting and diagenesis processes** is crucial for a better
64 exploration and production in carbonates. Urgonian microporous carbonates of Provence, are
65 made of facies and reservoir properties analogue to Middle East microporous carbonate
66 reservoirs (Thamama, Kharaib and Shuaiba Formations; Borgomano et al. 2002, 2013; Sallier
67 2005; Fournier et al. 2011; Leonide et al. 2012; Léonide et al. 2014). Although Urgonian
68 microporous carbonates of Provence are analogue to Middle East reservoirs, the analogy can
69 be extended to other faulted microporous carbonate reservoirs. To have a better comprehension
70 of diagenetic modifications linked to fault zones **in** these rocks, the aim of this paper is (i) to
71 determine the diagenetic evolution of polyphasic fault zones; (ii) to identify their impact on
72 reservoir properties and (iii) to link the fault evolution with the fluid flow and geodynamic
73 history of the basin.

74 **2. GEOLOGICAL CONTEXT**

75 We studied two faults cross-cutting microporous Valanginian-to-Early Aptian Urgonian
76 carbonates of the South-East Basin (Provence-SE France) deposited along the southern margin
77 of the Vocontian Basin (Léonide et al., 2014; Masse and Fenerci Masse, 2011). The “Urgonian”
78 platform carbonates (Masse, 1976) reached their maximum areal extension during the late
79 Hauterivian–Early Aptian (Masse and Fenerci-Masse, 2006). From Albian to Cenomanian, the
80 regional Durancian uplift triggered exhumation of Early Cretaceous carbonates, bauxitic
81 deposition (Guyonnet-Benaize et al., 2010; Lavenu et al., 2013; Léonide et al., 2014; Masse
82 and Philip, 1976; Masse, 1976), and development E-W-trending extensional faults (Guyonnet-
83 Benaize et al., 2010; Masse and Philip, 1976). During **Late Cretaceous** times, platform
84 environment led to a transgressive rudist deposition (Philip, 1970). From Late Cretaceous to
85 Eocene, the convergence between Iberia and Eurasia plates (e.g. Bestani 2015, and references
86 therein) caused a regional N-S shortening (e.g. Molliex et al. 2011 and references therein). The
87 so-called “Pyrénéo-Provençal” shortening, gave rise to E-W-trending north-verging thrust
88 faults and ramp folds (e.g. Bestani et al. 2016, and references therein). From Oligocene to
89 Miocene, the area underwent extension associated to Liguro-Provençal Basin opening (e.g.
90 Demory et al. 2011). During Mio-Pliocene times, the Alpine shortening dimly impacted the
91 studied area (Besson, 2005; Bestani, 2015), and reactivated the “Pyrénéo-Provençal” structures
92 (Champion et al., 2000; Molliex et al., 2011).

93 We studied two faults pertaining to a Km-scale fault system on the E-W-trending La Fare
94 anticline near Marseille (Fig. 1A). The southern limb of this anticline dips 25° S, and is
95 constituted by Upper Hauterivian, Lower Barremian and Santonian rocks (Fig. 1B). The Upper
96 Barremian carbonates are composed, from bottom to top, of a 120 m-thick calcarenitic unit
97 **with** cross-beddings, a 40 m-thick massive coral-rich calcarenite unit, and an upper 10 m-thick
98 calcarenite unit (Masse, 1976; Matonti et al., 2012; Roche, 2008). Santonian age coarse rudist
99 limestones uncomfortably overlap the Barremian carbonates (Fig. 1A).

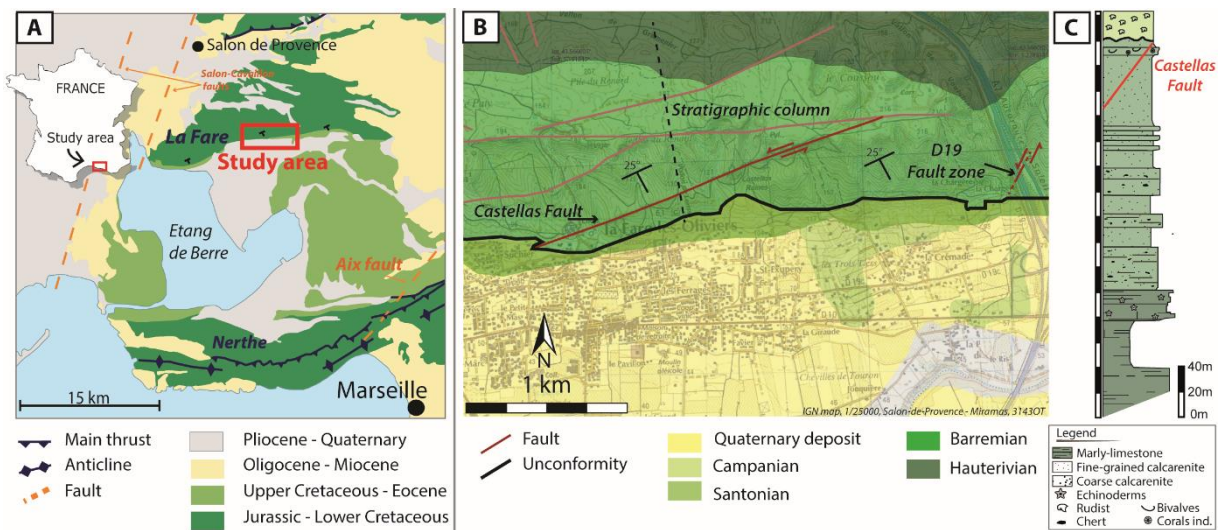
100 The Castellás fault zone is a 2.14 km-long left-lateral strike-slip fault, N060° to 070°-trending
 101 and 40° to 80°N-dipping (Fig. 2A, 2B; table 1) composed of horse structures, secondary faults
 102 and lenses (Fig. 2A, 2C; Aubert et al. (2019b)). The second investigated fault zone “D19” is
 103 composed of 5 sub-fault zones (F1 to F5) restricted in a 50 m-long interval (Fig. 2E, 2H; Table
 104 1; (Aubert et al., 2019a)). Sub-faults are organised into two sets. The first one comprises F3 and
 105 F4, N040 to N055-trending, 60-80°NW-dipping (orange traces on Fig. 2F). Set 2 is N030-
 106 trending, dipping 80°E, with left-lateral strike-slip slickensides pitch 20° to 28°SW (F1, F2, F5,
 107 red traces on Fig. 2F).

108

109 The internal structure of both fault zones results from three distinct tectonic events:

- 110 - the Durancian uplift dated as mid-Cretaceous leading to extension and to normal *en*
 111 *echelon* normal faults. The Castellás fault nucleated during this first extensional event
 112 and bears early dip-slip normal striations (Matonti et al., 2012),
- 113 - the Early Pyrenean compression with N000° to N170°-trending σ_H (see cited references
 114 in Espurt et al. 2012) which reactivated the Castellás fault as sinistral (Matonti et al.,
 115 2012) and led to the newly-formed strike-slip faults of the D19 outcrop (Aubert et al.,
 116 2019a).
- 117 - the Pyrenean to Alpine folding, triggering the 25°S tilting of the strata and fault zones.
 118 Faults of the D19 outcrop were reactivated while the Castellás fault tilting led to an
 119 apparent present-day reverse throw (Aubert et al., 2019a).

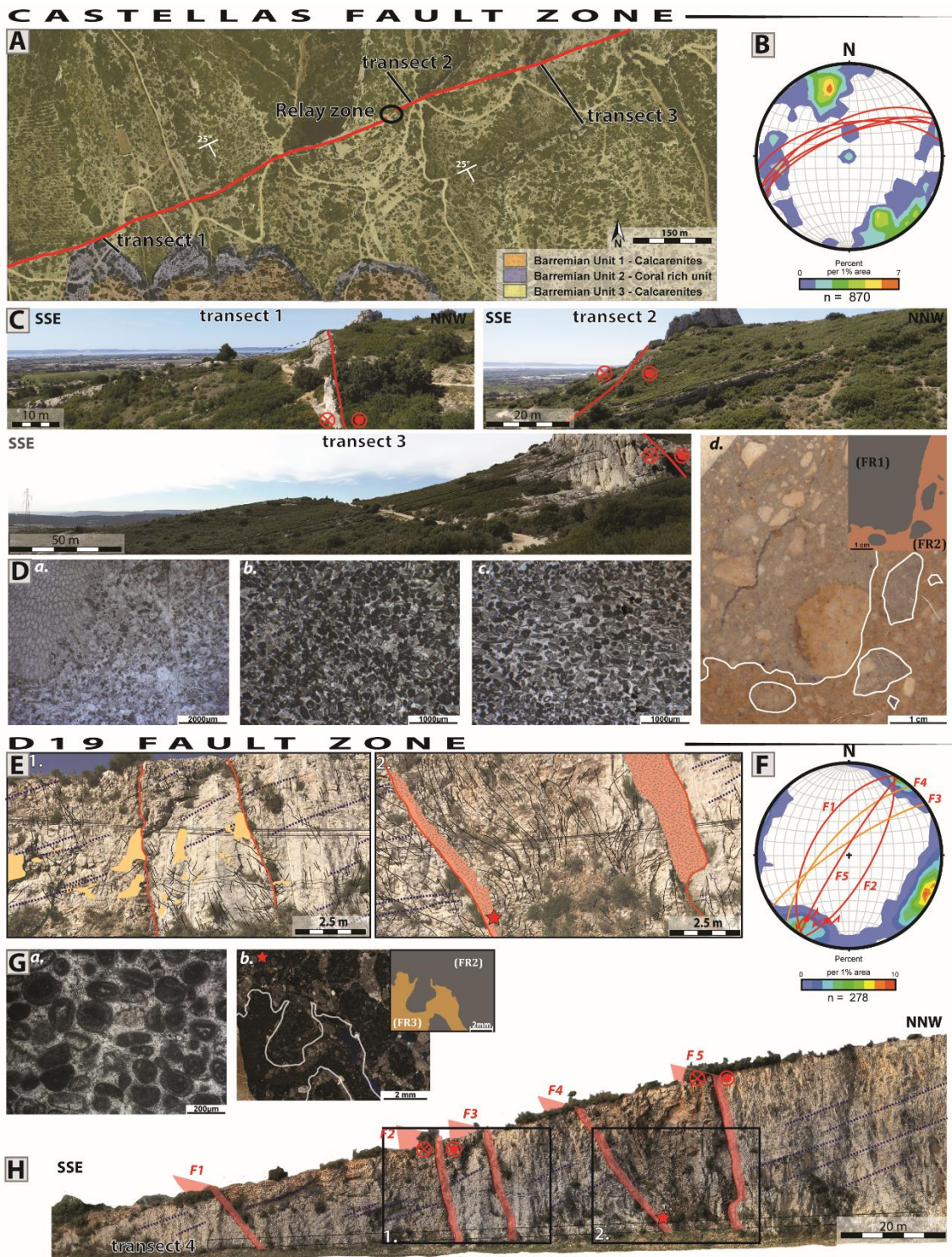
120



121

122 **Figure 1** : Geological context of the study area. A: geological map of Provence, B: Simplified structural map with the
 123 location of the Castellás fault and the stratigraphic column (black dashed line); C: Stratigraphic column of exposed
 124 Cretaceous carbonates (modified from Roche, 2008).

125



126

127 **Figure 2** : A: Castellás fault map on aerial photo with position of the studied transects and the relay zone; B: stereographic
 128 **projection** of poles to fractures (density contoured) and faults (red lines) (Allmendinger et al., 2013; Cardozo and
 129 Allmendinger, 2013); C: Photos of transects 1 to 3; D: Photomicrographs of carbonate host-rock facies (a) transect 1 coral
 130 rich unit, (b) transect 2 calcarenites, (c) transect 3 calcarenites and (d) fault rocks 1 and 2 (FR1 and FR2); E: Pictures of D19
 131 outcrop F: Stereographic **projection** of poles to fractures (density contoured), set one faults (orange line) and set 2 faults (red
 132 line) G: **Photomicrographs** of host rock facies (a) and of fault rocks (b; red stars on the pictures); H: D19 outcrop including
 133 the five faults F1 to F5.

134

Fault zones	Fault	Direction	Dip	Dip direction	Pitch striation	Fault core thickness	Fault Rocks		
							FR1	FR2	FR3
Castellas	Castellas	060 - 070	40 to 80	N	14 W -	0 to 4 m	sparsely present	majoritarily present	/
D19	F1	030	56	W		20	/	<10 cm	/
	F2	029	70	E	28 S	10 to 15	/	?	variable thickness
	F3	056	80	N		0 to 15	/	?	?
	F4	042	70	W		20	/	in the clasts of FR3	variable thickness
	F5	032	85	N	20 SW	50 to 100	/	/	variable thickness

136

137 3. DATA BASE

138 We performed 4 transects across the Castellas Fault and the D19 Fault (Fig. 2). Transect 1 is
 139 located along the coral rich unit 2. This lithostratigraphic unit is essentially composed of
 140 peloidal grains and bioclasts (corals, bivalves and stromatoporidae; Fig. 2Da). Transects 2 and
 141 3 cross-cut unit 3, made of fine calcarenites with peloidal grains and a rich fauna (foraminifera,
 142 bivalves, ostracods and echinoderms; Fig. 2Db, c). Transect 4 was conducted along the D19
 143 outcrop (Fig. 3), which exposes Barremian outer platform bioclastic calcarenite with current
 144 ripples. The grains are mainly peloids with minor amounts of bioclasts (solidary corals,
 145 bryozoans, bivalves and some rare miliolids; Fig. 2Ga).

146

147 The different tectonic events impacted the fault zone and fault core structure. Three different
 148 fault rock types were identified in the fault core of the two investigated fault zones (see Aubert
 149 et al. 2019a; Matonti et al., 2012). Fault rock 1 (FR1) results from the extensional activation of
 150 the Castellas fault during Durancian uplift. It is a cohesive breccia composed of sub-rounded to
 151 rounded clasts from the nearby damage zone and <30% of fine-grey matrix (Fig. 2Dd). Fault
 152 rock 2 (FR2), is linked to the strike-slip reactivation of the Castellas fault and to the onset of
 153 D19 fault zone during the Pyrenean shortening. FR2 presents two morphologies depending on
 154 the fault zones. Within Castellas fault, FR2 is an un-cohesive breccia with an orange/oxidized
 155 matrix with angular to sub-rounded clasts belonging to the nearby damage zone and from FR1
 156 (Fig. 2Dd). In the D19 fault zone, FR2 is a cohesive breccia with rounded clasts of the damage
 157 zone and a white cemented matrix (Fig. 2Gb). Fault rock 3 (FR3) is formed by the reactivation
 158 of D19 fault zone. The timing of D19 fault reactivation is tricky to determine as it can be related
 159 both to Pyrenean or alpine shortening. FR3 is composed of angular to sub-angular clasts from
 160 FR2 and from the nearby damage zone dispersed in an orange/oxidized matrix (<20%) (Fig.
 161 2Gb).

162

163 4. METHODS

164 The data set comprises 122 samples, 62 from Castellas and 60 from D19 outcrops, collected
 165 along the 4 transects. Porosity values were measured on 92 dry plugs with a Micromeritics
 166 AccuPyc 1330 helium pycnometer. Microfacies were determined on 92 thin sections.
 167 Impregnation with a blue-epoxy resin allowed us to decipher the different pore types. Thin
 168 sections were coloured with a solution of hydrochloric acid, Alizarin Red S and potassium
 169 ferricyanide to distinguish carbonate minerals (calcite and dolomite). Thin sections were
 170 analysed using cathodoluminescence to discriminate the different generations of calcite

171 cements. The paragenetic sequence was defined based on superposition and overlap principles
172 observed on thin sections using a Technosyn Cold Cathode Luminescence Model 8200 Mk II
173 coupled to an Olympus_BH2 microscope and to a Zeiss_MR C5. Micrite micro-fabric and
174 major element composition of two samples from the fault zone, two from the host rock and 1
175 from the D19 karst infilling were measured using PHILIPS XL30 ESEM with a beam current
176 set at 20 kV on fresh sample surfaces and on thin sections. To determine stable carbon and
177 oxygen isotopes ($\delta^{13}\text{C}$ and $\delta^{18}\text{O}$), 204 microsamples (<5 mg) were drilled, 194 of them were
178 micro-drilled from polished thin sections with an 80 μm diameter micro-sampler (Merkantec
179 Micromill) at the VU University (Amsterdam, The Netherlands). We micro-sampled bulk rocks
180 (57), sparitic cements (101), fault rocks (9) and micrite (27). The bulk rock values are related
181 to a non-selective sampling giving information on the whole rock isotopic values. These values
182 do not capture the signature of isolated cement (Swart, 2015). Carbon and oxygen isotopic
183 values were acquired with Thermo Finnigan Delta + mass spectrometer equipped with a
184 GASBENCH preparation device at VU University Amsterdam. The internationally used
185 standard IAEA-603, with official values of +2.46‰ for $\delta^{13}\text{C}$ and -2.37‰ for $\delta^{18}\text{O}$, is measured
186 as a control standard. The standard deviation (SD) of the measurements is respectively < 0.1‰
187 and < 0.2 ‰ for $\delta^{13}\text{C}$ and $\delta^{18}\text{O}$. Ten whole rock samples were analysed using a Gasbench II
188 connected to a Thermo Fisher Delta V Plus mass spectrometer at the FAU University (Erlangen,
189 Germany). Measurements were calibrated by assigning $\delta^{13}\text{C}$ values of +1.95‰ to NBS19 and
190 -47.3‰ to IAEA-CO9 and $\delta^{18}\text{O}$ values of -2.20‰ to NBS19. All values are reported in per mil
191 relative to V-PDB.

192 5. RESULTS

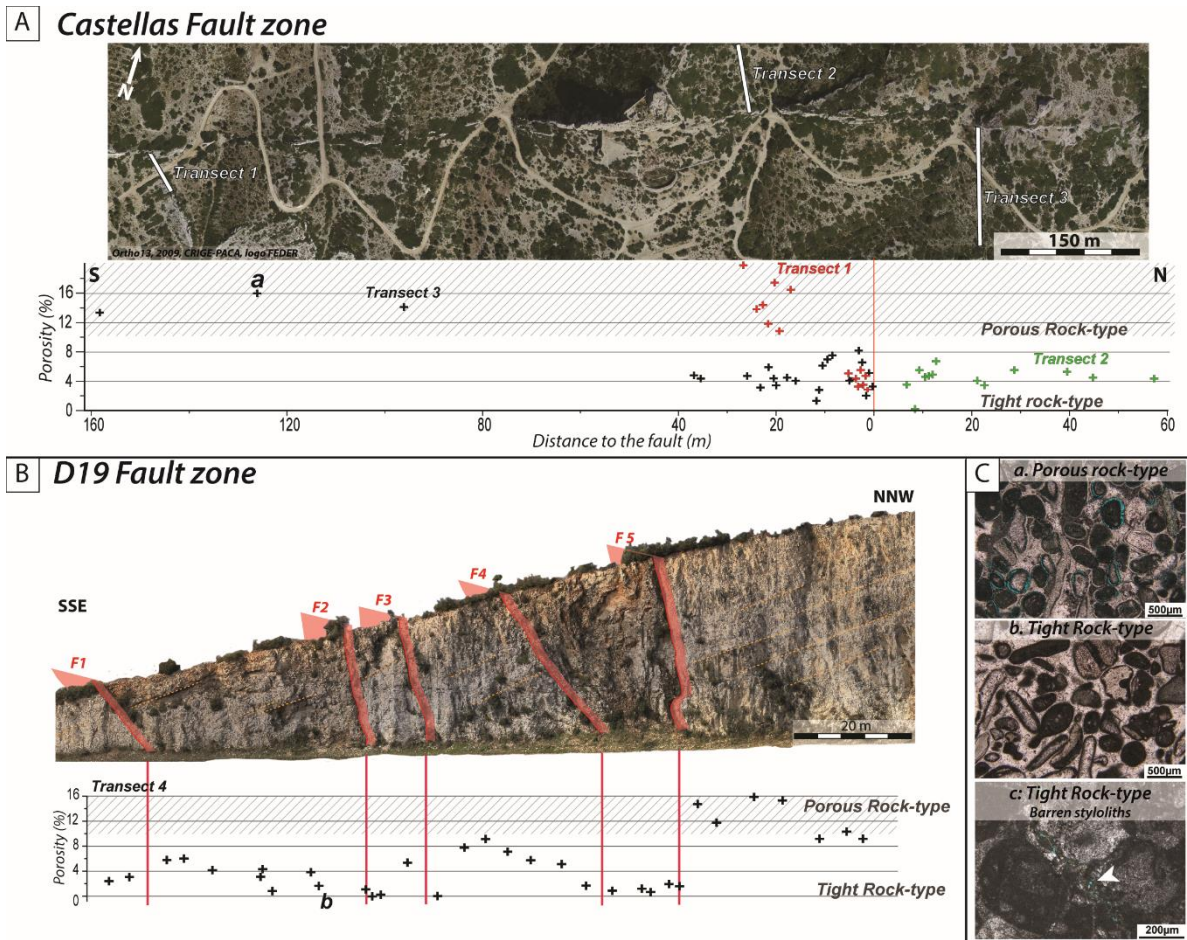
193 1. MICROPOROSITY AND POROSITY

194 Porosities **measured on** the 92 samples show a strong decrease towards the fault core (Fig. 3):
195 dropping from more than 10% in the host carbonates (mean: 15%, SD: 2.68 for Castellás and
196 mean: 12.3%, SD: 2.52 for D19) to less than 5% within fault zones (mean: 4.8%, SD: 2.07 for
197 Castellás and mean: 3.16%, SD: 2.35 for D19).

198 Along transects, some porosity variations occur as follows:

- 199 - North of the Castellás fault, along the 60 m-long transect 2 the porosity is constantly
200 lower than 7% (mean of 4.4%, SD: 1.53; Fig. 3A).
- 201 - South of the Castellás fault, the reduced porosity zone is wider than 40 m in transect 3
202 and 30 m in transect 1 (Fig. 3A). In a 10 m-thick zone from the fault plane, porosity
203 reduction occurs with lower values in transect 1 (average 4.9%) than in transect 3
204 (average 5.6%).
- 205 - In the D19 fault zone, the lowest porosity values are found in narrow zones around the
206 faults (less than 2 m-wide) and in the lens between F4 and F5. Though, this porosity
207 decrease is not homogeneous in fault zone and high values are found north of F1 and
208 F3 (Fig. 3B).

209



210

211 **Figure 3:** A: Castellás fault zone aerial view (Ortho13, 2009, CRIGE-PACA, logo FEDER) and porosity values measured
 212 along transect 1 (red Cross), transect 2 (green cross) and transect 3 (black cross); B: porosity values measured along D19
 213 fault zone; C: Pore types in the host rock (a) and in the fault zones (b and c).

214 Microscope observation of thin sections impregnated with blue-epoxy resin allowed to identify
 215 a porous rock-type with $\phi > 10\%$ mainly in micritized grains as microporosity and moldic
 216 porosity (Fig. 3Ca), and a tight rock-type with $\phi < 5\%$, where the porosity is mostly linked to
 217 barren stylolites (Fig. 3Cb, c).

218 2. DIAGENETIC PHASES

219 a. Micrite micro-fabric

220 Micritised bioclasts, ooids and peloids were observed after SEM analysed of two fault zones
 221 samples and two host rock samples. Two micro-fabrics of micrite occur with specific crystal
 222 shape, sorting and contacts according to Fournier et al. (2011). Within both fault zones, the
 223 micrite is tight, with compact subhedral mosaic crystals less than $10\ \mu\text{m}$ -wide (MF1; Fig. 4A,
 224 B). In the host rock, the micrite is loosely packed, and partially coalescent with punctate rarely
 225 serrate, subhedral to euhedral crystals less than $5\ \mu\text{m}$ -wide (MF3; Fig. 4C, D, E). MF1 correlates
 226 with low porosity values ($< 5\%$), while MF3 with higher porosity ($> 10\%$).

227 b. Diagenetic cements

228 Eight different cement stages were identified (Fig. 5). The red stain links to Alizarin Red S
 229 coloration and shows that all visible cements are made of calcite, which exhibits variable
 230 characteristics (morphology, luminescence, size and location).

231 The first two cement phases occur in both fault zones. The first cement (C0) is non-luminescent
232 isopachous calcite of constant thickness (~10 μm) around grains (Fig. 5A). The second cement
233 (C1) is divided in two sub-phases: a non-luminescent calcite, C1a, with a crystal size ranging
234 from 50 μm to more than 200 μm , a dog-tooth morphology in intergranular spaces, and a bright
235 luminescence calcite, C1b, covering C1a with a maximum thickness of 100 μm (Fig. 5A, B,
236 D, G). C1b also fills micro-porosity in micritised grains (Fig. 5B). C1b areal occurrence
237 strongly increases in Castellás fault zone.

238

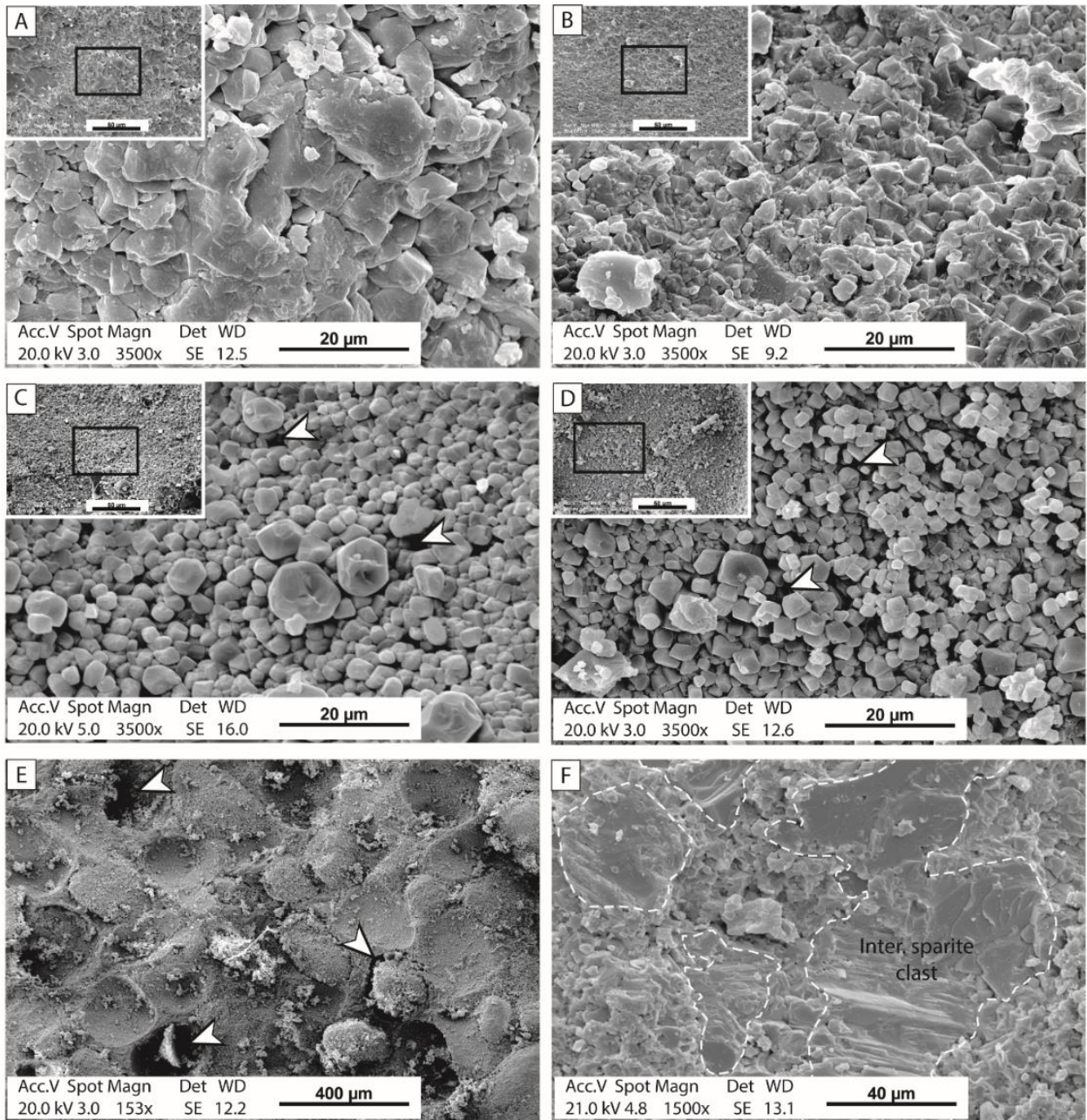


Figure 4 : MEB pictures of micrite micro-fabric and microporosity (white arrows); A. MF1 micrite micro-fabric in Castellás fault zone (2.5 m to fault plane); B. MF1 micrite micro-fabric within D19 fault zones (2 m away from F5 fault plane); C. MF3 micrite micro-fabric within Castellás host rock (188 m away from the fault plane); D. MF3 micrite micro-fabric within D19 host rock (95 m away from F5 fault plane); E. D19 host rock moldic porosity; F. Karst infilling.

239 Five cements or replacive phases extensively occur in the Castellás sector and rarely in the D19
 240 outcrop:

- 241 - C2 is a sparitic cement, with dull-orange luminescent crystals with a maximum size of
 242 100 µm only found in veins of the fault core (Fig. 5B). SEM measurements show the
 243 presence of Si and Al in the C2 veins. Most of Si crystals are automorphic and have
 244 black luminescence.

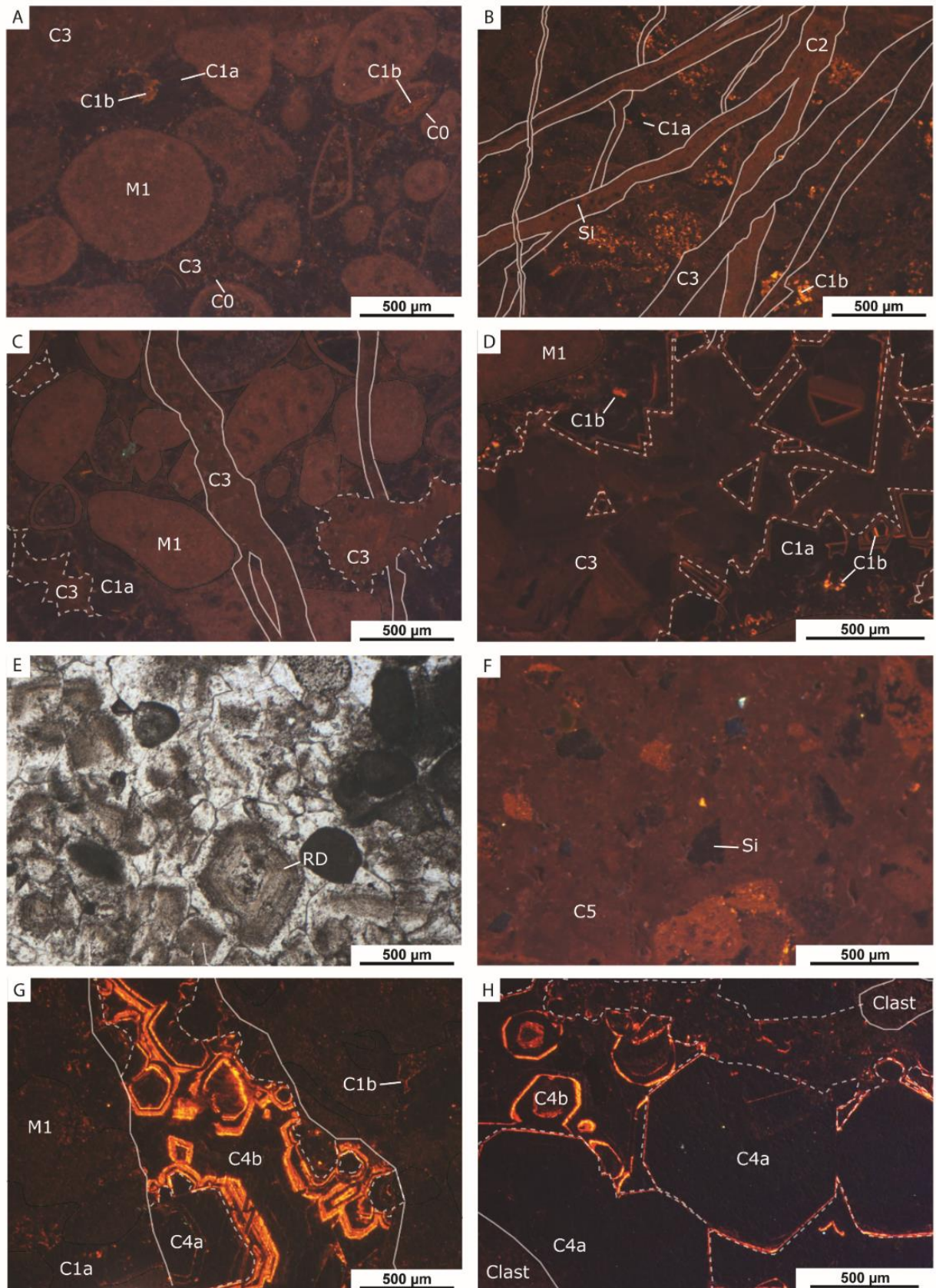


Figure 5 : Thin-sections under cathodoluminescence; A: Calcarenite in transect 3 with micritised grain (M1), and intergranular volume cemented with C1 a and b and C3; B: C2 (with Si) and C3 veins affecting Castellans FR1 clasts with micritised grains cemented by C1b; C: C3 veins, cements and intergranular volumes in Castellans fault zone; D: C1 (a and b) and C3 cementing moldic porosity of transect 3 calcarenite; E: FR1 matrix with phantom of cloudy appearance replacive dolomite (RD); F: FR1 matrix de-dolomitized by C5 containing quartz grains; G: C4 (a and b) cementing vein of D19 fault zone; H: matrix of D19 FR2 cemented by C4 (a and b).

- 246 - C3 is a blocky calcite with non to red-dull luminescence in veins, moldic and
247 intergranular pores (Fig. 5B, C, D). This cement also occurs in few veins of D19 sectors
248 but is not restricted only to the fault zone.
- 249 - Phantoms of planar-e (euhedral) dolomite crystals (Sibley and Gregg, 1987) with a
250 maximum size of 500 μm affect the matrix of FR1 (Fig. 5E). They are vestiges of a
251 previous dolomitization phase. They have a cloudy appearance caused by solid micritic
252 inclusion inside crystals and can be considered as replacive dolomite (RD; Machel,
253 2004). Within the FR1 matrix, an important concentration of angular grains of quartz
254 with a maximum size of 300 μm is noticed (Fig. 5F).
- 255 - A blocky calcite C4 (referred to as S2 in Aubert et al. (2019a)) is mainly present in veins
256 of the D19 outcrop, in matrix of FR2, and intergranular and moldic pores (Fig. 5G, H).
257 This cement shows zonations of non-luminescent and bright luminescent bands and can
258 be divided in two sparitic sub-phases: C4a which is non-luminescent with some highly
259 luminescent bands while C4b is bright luminescent with some thin non-luminescent
260 zones. C4a occurs in lesser proportion in some veins along transect 2 and 3 of the
261 Castellás fault.
- 262 - A sparitic cement C5, with a red-dull luminescence replaces the RD phase (Fig. 5F).

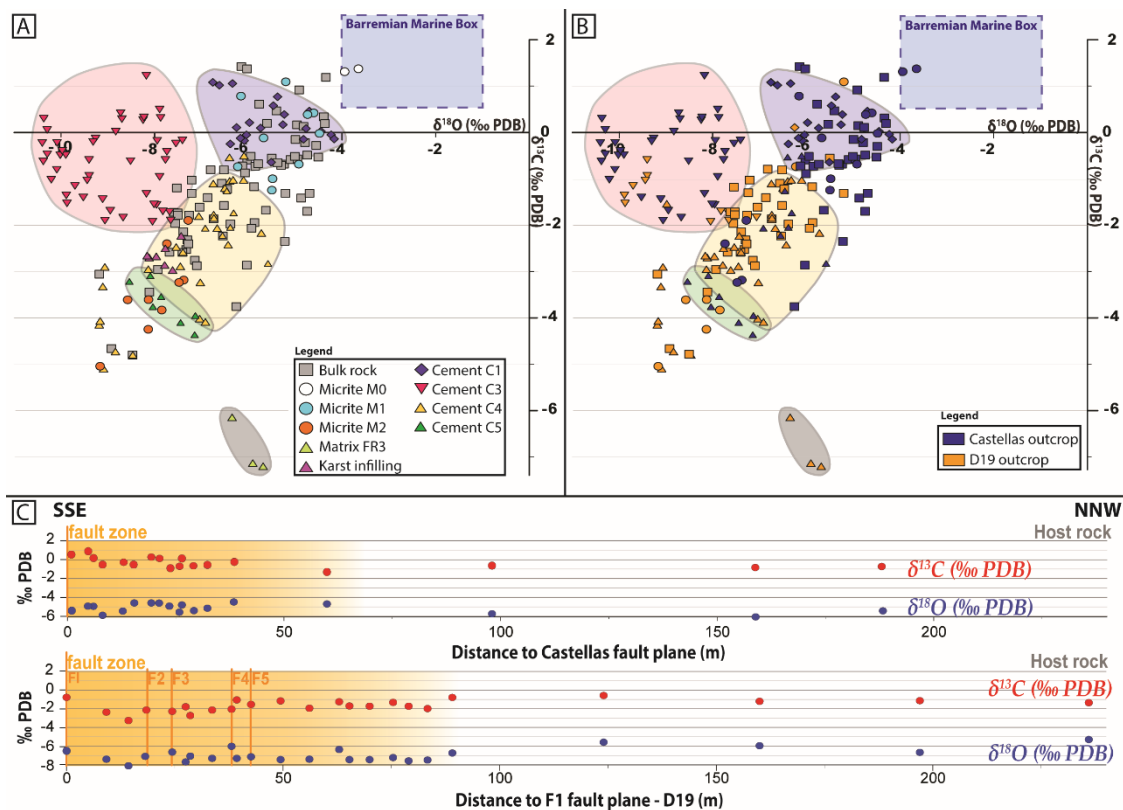
263 c. Additional diagenetic features

264 In addition to cementation phases, other diagenetic elements affected both fault zones. Karst
265 infilling occurs in the F2 fault zone of the D19 outcrop. It is composed of well-sorted grains
266 deposited in laminated layers. This karst deposit presents a stack of alternating micrite-rich and
267 grain-rich layers from the latter composed of former blocky calcite belonging to dissolved
268 grainstones. The laminated layers are affected by veins and stylolites; some of these are
269 deformed due to the grain fall on sediments. Micritic layers have been observed under SEM,
270 and the micrite appears tight with compact subhedral mosaic crystals (Fig. 4F). We observed
271 oxide filling mainly in the Castellás area in dissolution voids affecting C1a, C1b and C3
272 cementation phases and in D19 in karstic fill. The areal amount of oxides increases close to
273 stylolites.

274 3. CARBON AND OXYGEN ISOTOPES

275 Isotope measurements were realized on samples collected along transects of the fault zones. A
276 hundred and eighty-nine measurements of C and O isotopes were performed on 16 samples and
277 32 thin sections (Fig. 6A, table 2).

278 Sampling was done in bulk rock (66), sparitic cement (101; veins, intergranular volume and
279 fault rock cements) and in fault rocks (10) in order to determine their isotopic signature. Isotopic
280 values range from -10.40‰ to -3.65‰ for $\delta^{18}\text{O}$ and from -7.20‰ to +1.42‰ for $\delta^{13}\text{C}$ (Fig. 6A,
281 B, table 2). The bulk rock values range from -9.18‰ to -4.34‰ for $\delta^{18}\text{O}$ and from -4.80‰ to
282 +1.19‰ for $\delta^{13}\text{C}$ (Fig. 6A, table 2). These values are split in two sets. Set 1 includes transects
283 1 and 3 of the Castellás Fault. Bulk values range from -6.07‰ to -4.34‰ for $\delta^{18}\text{O}$ and from -
284 1.41‰ to +1.19‰ for $\delta^{13}\text{C}$. Set 2 includes transects 2 (Castellás) and 4 (D19). Bulk values
285 range from -9.18‰ to -5.20‰ for $\delta^{18}\text{O}$ and from -4.80‰ to -0.60‰ for $\delta^{13}\text{C}$ (Fig. 6B, table 2).
286 In transect 3, the isotopic values only slightly vary, ranging from -6.13‰ to -4.50‰ for $\delta^{18}\text{O}$
287 and from -1.41‰ to +0.47‰ for $\delta^{13}\text{C}$ respectively (Fig. 6C, table 2). On the contrary, values
288 are more variable along the D19 transect; they range from -9.18‰ to -5.20‰



290

291 **Figure 6** : Isotopic values of $\delta^{13}\text{C}$ and $\delta^{18}\text{O}$ measured on bulk rock, cement phases, and micrite. Range values of “Urgonian
 292 marine box” from Moss & Tucker (1995) and Godet et al. (2006); A: set of values sorted by the nature of diagenetic phases
 293 and B: values sorted by the fault zone; C: lateral evolution of $\delta^{13}\text{C}$ and $\delta^{18}\text{O}$ bulk isotopic values in Castellás (top) and in D19
 294 (bottom) fault zones.

295 for $\delta^{18}\text{O}$ and from -4.80‰ to -0.60‰ for $\delta^{13}\text{C}$ (Fig. 6C, table 2). The $\delta^{13}\text{C}$ values are more
 296 depleted approaching to faults, especially south of F2.

297 Isotopic values of cements filling veins, intergranular volumes, karst infillings, and fault rocks
 298 are divided into 5 groups (Fig. 6A, table 2):

- 299 - Isotopic values of C1 cement fluctuate from -6.76‰ to -4.45‰ for $\delta^{18}\text{O}$ and from -1.28
 300 to $+1.08\text{‰}$ for $\delta^{13}\text{C}$;
- 301 - Isotopic values of C3 cement range from -10.40‰ to -6.73‰ for $\delta^{18}\text{O}$ and from -2.09
 302 to $+1.22\text{‰}$ for $\delta^{13}\text{C}$;
- 303 - Isotopic values of C4 cement in FR1 and FR2 matrix and in karst infillings range from
 304 -9.18‰ to -4.60‰ for $\delta^{18}\text{O}$ and from -5.10‰ to -0.74‰ for $\delta^{13}\text{C}$ with a positive
 305 covariance between $\delta^{18}\text{O}$ and $\delta^{13}\text{C}$. FR2 matrix values (from -7.06‰ to -6.55‰ for $\delta^{18}\text{O}$
 306 and from -1.10 to -2.24‰ for $\delta^{13}\text{C}$) present slightly less depleted values than karst
 307 infillings with mean values of -7.83‰ and -2.53‰ for $\delta^{18}\text{O}$ and $\delta^{13}\text{C}$ respectively. (Fig.
 308 6A). In the Castellás fault, 4 isotopic values from two veins are enriched with means of
 309 -6.25 and -4.2‰ for $\delta^{18}\text{O}$ -0.64 and -0.09‰ for $\delta^{13}\text{C}$ having similar positive covariance
 310 than the other C4 values;
- 311 - Isotopic values of C5 cement, sampled in FR1 matrix display mean of -7.49‰ for $\delta^{18}\text{O}$
 312 and -4.01‰ for $\delta^{13}\text{C}$ (Fig. 6A);

313 - Isotopic values of FR3 matrix with a mean of -5.98‰ for $\delta^{18}\text{O}$ and -6.83‰ for $\delta^{13}\text{C}$
 314 (Fig. 6A).

315

316 **Table 2:** Carbon and oxygen isotope values of bulk carbonates for Castellás fault zone and D19
 317 fault zones. *B:* bulk measurement; *M:* micrite value; *C1, C3, C4, C5:* cement isotopic value;
 318 *FR:* fault rock isotopic value.

Transect	Sample	$\delta^{13}\text{C}$ (‰VPDB)	$\delta^{18}\text{O}$ (‰VPDB)	Class	Distance to F. (m)
Transect 1 (Cast.)	201	1,19	-4,34	B	1,3
Transect 1 (Cast.)	201	1,02	-6,62	C1	1,3
Transect 1 (Cast.)	201	1,31	-3,94	M	1,3
Transect 1 (Cast.)	201	1,37	-3,65	M	1,3
Transect 1 (Cast.)	213	-0,68	-5,24	B	22,7
Transect 1 (Cast.)	213	-0,58	-5,10	B	22,7
Transect 1 (Cast.)	213	-0,18	-6,09	C1	22,7
Transect 1 (Cast.)	213	0,03	-4,45	C1	22,7
Transect 1 (Cast.)	213	0,09	-4,77	C1	22,7
Transect 1 (Cast.)	213	-2,09	-6,92	C4	22,7
Transect 1 (Cast.)	213	-0,68	-4,92	M	22,7
Transect 2 (Cast.)	c3b17	-0,52	-5,95	B	4,6
Transect 2 (Cast.)	c3b17	-2,07	-6,38	C4	4,6
Transect 2 (Cast.)	c3b7	-0,64	-5,51	B	9,3
Transect 2 (Cast.)	c3b26	-3,76	-6,26	B	22,6
Transect 2 (Cast.)	c3b26	-2,85	-5,58	C4	22,6
Transect 2 (Cast.)	c3b26	-1,31	-4,69	B	57,3
Transect 2 (Cast.)	c3b7	-1,76	-6,31	C1	57,3
Transect 2 (Cast.)	c3b7	-1,28	-6,46	C1	57,3
Transect 2 (Cast.)	c3b26	-2,35	-5,22	M	57,3
Transect 2 (Cast.)	c3b26	-1,70	-4,75	M	57,3
Transect 3 (Cast.)	327	-0,24	-7,55	C3	0,3
Transect 3 (Cast.)	325	-1,90	-9,06	C3	0,3
Transect 3 (Cast.)	325	-1,69	-8,95	C3	0,3
Transect 3 (Cast.)	327	-3,11	-8,09	C4	0,3
Transect 3 (Cast.)	327	0,47	-5,40	B	1,0
Transect 3 (Cast.)	327	-0,18	-7,95	C3	1,0
Transect 3 (Cast.)	327	-0,17	-7,41	C3	1,0
Transect 3 (Cast.)	328	0,10	-5,74	C1	1,6
Transect 3 (Cast.)	328	-1,32	-8,18	C3	1,6
Transect 3 (Cast.)	328	-0,59	-7,77	C3	1,6
Transect 3 (Cast.)	328	-0,42	-7,74	C3	1,6
Transect 3 (Cast.)	328	-0,13	-9,26	C3	1,6
Transect 3 (Cast.)	328	0,02	-8,83	C3	1,6

Transect 3 (Cast.)	328	0,29	-8,70	C3	1,6
Transect 3 (Cast.)	328	0,42	-8,73	C3	1,6
Transect 3 (Cast.)	328	0,50	-7,89	C3	1,6
Transect 3 (Cast.)	328	1,22	-8,18	C3	1,6
Transect 3 (Cast.)	333	-1,84	-8,67	C3	1,6
Transect 3 (Cast.)	333	-0,96	-7,89	C3	1,6
Transect 3 (Cast.)	328	-0,14	-4,17	C4	1,6
Transect 3 (Cast.)	328	-0,05	-4,23	C4	1,6
Transect 3 (Cast.)	329	0,16	-4,95	B	2,4
Transect 3 (Cast.)	333	-0,25	-6,38	C1	4,6
Transect 3 (Cast.)	333	-0,12	-6,17	C1	4,6
Transect 3 (Cast.)	333	-0,62	-8,52	C3	4,6
Transect 3 (Cast.)	333	-0,12	-5,67	M	4,6
Transect 3 (Cast.)	333	-0,02	-4,48	M	4,6
Transect 3 (Cast.)	333	0,42	-4,60	M	4,6
Transect 3 (Cast.)	337	0,19	-5,59	B	9,5
Transect 3 (Cast.)	302	-0,53	-4,50	B	11,8
Transect 3 (Cast.)	302	-0,49	-4,74	B	11,8
Transect 3 (Cast.)	302	-0,62	-10,38	C3	11,8
Transect 3 (Cast.)	302	-0,49	-10,02	C3	11,8
Transect 3 (Cast.)	305	0,33	-4,38	B	16,0
Transect 3 (Cast.)	306	0,21	-4,35	B	17,8
Transect 3 (Cast.)	307	-0,01	-4,46	B	18,2
Transect 3 (Cast.)	308	-0,57	-4,95	B	20,0
Transect 3 (Cast.)	308	-1,44	-9,11	C3	20,0
Transect 3 (Cast.)	308	-0,23	-10,40	C3	20,0
Transect 3 (Cast.)	308	-0,22	-10,08	C3	20,0
Transect 3 (Cast.)	309	-1,41	-4,87	B	20,5
Transect 3 (Cast.)	309	-0,52	-5,01	B	20,5
Transect 3 (Cast.)	309	-0,15	-4,82	C1	20,5
Transect 3 (Cast.)	309	-1,56	-7,96	C3	20,5
Transect 3 (Cast.)	309	-1,55	-8,01	C3	20,5
Transect 3 (Cast.)	312	0,12	-4,81	B	23,2
Transect 3 (Cast.)	314	-0,71	-5,30	B	25,9
Transect 3 (Cast.)	314	-0,80	-10,09	C3	25,9
Transect 3 (Cast.)	314	-0,49	-9,90	C3	25,9
Transect 3 (Cast.)	314	-0,47	-10,29	C3	25,9
Transect 3 (Cast.)	314	-0,40	-9,97	C3	25,9
Transect 3 (Cast.)	314	0,06	-10,30	C3	25,9
Transect 3 (Cast.)	316	-1,24	-5,50	B	29,2
Transect 3 (Cast.)	316	-1,00	-5,48	B	29,2
Transect 3 (Cast.)	316	-0,22	-4,79	B	29,2
Transect 3 (Cast.)	316	-1,02	-10,21	C3	29,2
Transect 3 (Cast.)	316	-0,18	-9,31	C3	29,2
Transect 3 (Cast.)	316	0,30	-10,37	C3	29,2
Transect 3 (Cast.)	318	-0,28	-4,53	B	35,4

Transect 3 (Cast.)	320	-0,68	-5,79	B	96,1
Transect 3 (Cast.)	322	-0,88	-6,07	B	158,0
Transect 3 (Cast.)	323	-0,65	-5,37	B	188,0
Castellas (ZF1)	Z1,1	0,17	-5,26	C1	0,0
Castellas (ZF1)	Z1,1	0,39	-5,23	C1	0,0
Castellas (ZF1)	Z1,1	0,46	-4,70	C1	0,0
Castellas (ZF1)	Z1,2	0,21	-5,98	C1	0,0
Castellas (ZF1)	Z1,1	-0,55	-6,40	C4	0,0
Castellas (ZF1)	Z1,1	-0,52	-6,10	C4	0,0
Castellas (ZF1)	Z1,2	-4,12	-7,45	C5	0,0
Castellas (ZF1)	Z1,2	-0,15	-4,99	FR	0,0
Castellas (ZF1)	Z1,2	0,39	-4,73	M	0,0
Castellas (ZF1)	Z1,2	0,61	-5,77	M	0,0
Castellas (ZF1)	Z1,1	0,78	-6,16	M	0,0
Castellas (ZF2)	Z2,2	0,77	-5,38	C1	0,0
Castellas (ZF2)	Z2,7	-1,40	-9,52	C3	0,0
Castellas (ZF2)	Z2,7	-4,38	-7,15	C5	0,0
Castellas (ZF2)	Z2,7	-3,97	-7,13	C5	0,0
Castellas (ZF2)	Z2,7	-3,78	-8,04	C5	0,0
Castellas (ZF2)	Z2,7	-3,56	-7,86	C5	0,0
Castellas (ZF2)	Z2,7	-3,24	-7,48	C5	0,0
Castellas (ZF2)	Z2,7	-3,23	-8,54	C5	0,0
Castellas (ZF2)	Z2,2	0,58	-5,47	FR	0,0
Castellas (ZF2)	Z2,2	0,92	-4,91	FR	0,0
Castellas (ZF2)	Z2,7	-1,68	-5,63	FR	0,0
Castellas (ZF2)	Z2,7	-2,24	-6,55	FR	0,0
Castellas (ZF2)	Z2,7	-3,18	-7,38	M	0,0
Castellas (ZF2)	Z2,7	-2,86	-6,03	FR	1,0
Castellas (ZF5)	Z5,4	0,27	-8,25	C3	0,0
Castellas (ZF5)	Z5,4	0,31	-7,87	C3	0,0
Castellas (ZF5)	Z5,4	0,32	-8,23	C3	0,0
Castellas (ZF5)	Z5,4	1,06	-6,34	C1	0,4
Castellas (ZF5)	Z5,4	1,08	-6,76	C1	0,4
Castellas (ZF5)	Z5,4	1,05	-7,13	FR	0,4
Castellas (ZF5)	Z5,4	1,37	-6,03	FR	0,4
Castellas (ZF5)	Z5,4	1,42	-6,15	FR	0,4
Transect	Sample	$\delta^{13}\text{C}$ (‰VPDB)	$\delta^{18}\text{O}$ (‰VPDB)	Class	Distance to F1 (m)
Transect 4 (D19)	3B	-0,81	-6,52	B	0,0
Transect 4 (D19)	3B	-1,20	-6,50	C1	0,0
Transect 4 (D19)	3B	-1,02	-6,33	C1	0,0
Transect 4 (D19)	3B	0,11	-6,25	C1	0,0
Transect 4 (D19)	3B	-0,74	-6,23	M	0,0
Transect 4 (D19)	9	-2,32	-7,30	B	9,2

Transect 4 (D19)	13a	-3,44	-8,11	B	14,3
Transect 4 (D19)	13a	-2,96	-7,93	B	14,3
Transect 4 (D19)	13C	-2,97	-7,62	M	14,3
Transect 4 (D19)	13C	-2,86	-7,79	M	14,3
Transect 4 (D19)	13C	-2,70	-8,12	M	14,3
Transect 4 (D19)	13C	-2,67	-7,96	M	14,3
Transect 4 (D19)	13C	-2,66	-8,16	M	14,3
Transect 4 (D19)	13C	-2,50	-7,77	M	14,3
Transect 4 (D19)	13C	-1,54	-8,98	M	14,3
Transect 4 (D19)	17	-2,58	-7,68	B	18,7
Transect 4 (D19)	14A	-1,97	-6,38	B	18,7
Transect 4 (D19)	14A	-1,87	-6,74	B	18,7
Transect 4 (D19)	15B	-2,23	-7,43	B	18,7
Transect 4 (D19)	17	-1,05	-6,40	C1	18,7
Transect 4 (D19)	14A	-1,77	-6,74	C1	18,7
Transect 4 (D19)	14A	-2,42	-6,43	C4	18,7
Transect 4 (D19)	14A	-2,06	-6,67	C4	18,7
Transect 4 (D19)	21	-2,23	-6,54	B	24,4
Transect 4 (D19)	RSG	-1,90	-7,66	B	28,4
Transect 4 (D19)	RSG	-1,70	-7,83	B	28,4
Transect 4 (D19)	RSD	-2,87	-7,10	B	29,5
Transect 4 (D19)	RSD	-2,76	-7,14	B	29,5
Transect 4 (D19)	RSD	-0,93	-9,40	C3	29,5
Transect 4 (D19)	RSF1	-2,40	-7,28	B	34,7
Transect 4 (D19)	RSF2	-2,14	-7,39	B	34,7
Transect 4 (D19)	RSF2	-1,78	-7,27	B	34,7
Transect 4 (D19)	RSF1	-1,03	-9,44	C3	34,7
Transect 4 (D19)	RSF2	-1,93	-8,05	C3	34,7
Transect 4 (D19)	RSF2	-0,59	-9,40	C3	34,7
Transect 4 (D19)	RSF2	-2,95	-8,14	C4	34,7
Transect 4 (D19)	RSE 1	-2,53	-7,33	B	35,0
Transect 4 (D19)	RSE 2	-2,59	-7,41	B	35,0
Transect 4 (D19)	RSE 1	-1,71	-7,68	C3	35,0
Transect 4 (D19)	RSE 2	-1,84	-6,73	C3	35,0
Transect 4 (D19)	57	-2,07	-5,93	B	38,1
Transect 4 (D19)	57	-1,94	-5,87	B	38,1
Transect 4 (D19)	57	-1,83	-7,06	C3	38,1
Transect 4 (D19)	57	-1,10	-6,75	C3	38,1
Transect 4 (D19)	57	-4,02	-7,04	C4	38,1
Transect 4 (D19)	57	-2,17	-5,72	C4	38,1
Transect 4 (D19)	57	-1,58	-6,52	FR	38,1
Transect 4 (D19)	57	-7,20	-5,68	M	38,1
Transect 4 (D19)	57	-7,13	-5,90	M	38,1
Transect 4 (D19)	28b	-1,03	-7,21	B	39,3
Transect 4 (D19)	28b	-1,03	-6,10	C3	39,3
Transect 4 (D19)	28b	-4,09	-6,92	C4	39,3

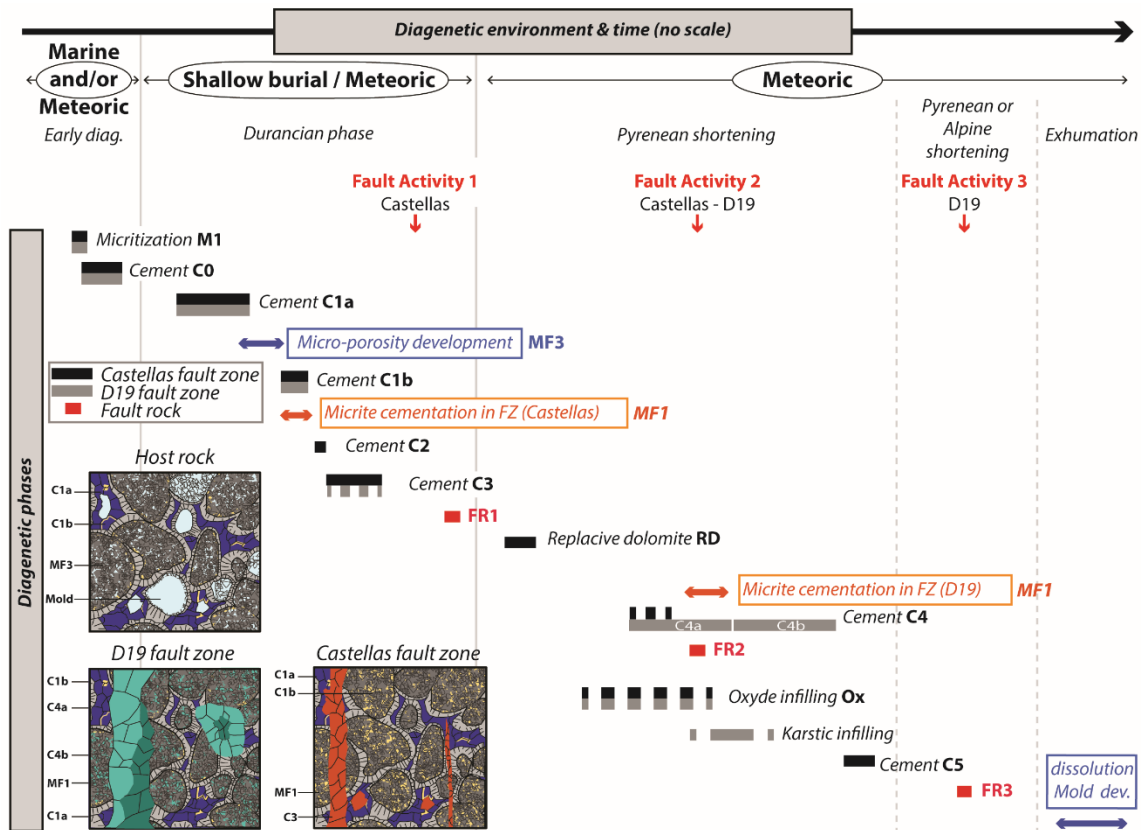
Transect 4 (D19)	28b	-2,58	-7,40	C4	39,3
Transect 4 (D19)	28b	-2,47	-7,54	C4	39,3
Transect 4 (D19)	30a	-1,61	-7,04	B	42,6
Transect 4 (D19)	30a	-1,41	-6,87	B	42,6
Transect 4 (D19)	30a	-3,23	-7,03	C4	42,6
Transect 4 (D19)	30a	-2,89	-7,45	C4	42,6
Transect 4 (D19)	24a	-1,21	-7,52	B	51,1
Transect 4 (D19)	27b	-1,92	-7,48	B	57,9
Transect 4 (D19)	31	-1,24	-6,44	B	65,0
Transect 4 (D19)	32	-1,75	-7,50	B	67,4
Transect 4 (D19)	34	-1,79	-7,49	B	72,2
Transect 4 (D19)	36	-1,32	-7,21	B	77,8
Transect 4 (D19)	38	-1,73	-7,59	B	81,5
Transect 4 (D19)	62	-1,96	-7,56	B	86,0
Transect 4 (D19)	42	-0,81	-6,80	B	91,9
Transect 4 (D19)	63	-0,55	-5,50	B	124,0
Transect 4 (D19)	64	-1,17	-5,88	B	160,0
Transect 4 (D19)	65	-1,10	-6,57	B	197,0
Transect 4 (D19)	66	-1,31	-5,21	B	236,0
Transect 4 (D19)	60a	-3,06	-9,18	B	255,2
Transect 4 (D19)	60B	-4,80	-8,47	B	255,2
Transect 4 (D19)	60B	-4,66	-8,92	B	255,2
Transect 4 (D19)	61	-1,53	-9,87	C3	255,2
Transect 4 (D19)	61	-1,36	-9,89	C3	255,2
Transect 4 (D19)	60a	-1,15	-9,70	C3	255,2
Transect 4 (D19)	60a	-3,32	-9,11	C4	255,2
Transect 4 (D19)	60B	-5,10	-9,09	C4	255,2
Transect 4 (D19)	60B	-4,73	-8,84	C4	255,2
Transect 4 (D19)	60B	-4,15	-9,18	C4	255,2
Transect 4 (D19)	60B	-4,07	-9,16	C4	255,2
Transect 4 (D19)	60B	-2,90	-9,06	C4	255,2
Transect 4 (D19)	60a	-3,83	-7,85	M	255,2
Transect 4 (D19)	60B	-5,04	-9,17	M	255,2
Transect 4 (D19)	60B	-4,25	-8,14	M	255,2
Transect 4 (D19)	60B	-3,61	-8,58	M	255,2
Transect 4 (D19)	60B	-3,61	-8,13	M	255,2

319 6. DISCUSSION

320 1. DIAGENETIC EVOLUTION OF THE FAULT ZONES

321 The chronological relations between cements can be established via cross-cutting relations and
322 inclusion principles. Indeed, the veins filled with C2 cement cross-cut C1a and C1b cements
323 (Fig. 5B). Thus, C2 cementation post-dated C1 cement. C3 veins cross-cut the C2 veins, but
324 are included within FR1 clasts (Fig. 5B). Hence, C3 cement is prior to FR1 development but is
325 subsequent to C2 cementation. The fault rock 1 (FR1) is related to the first extensional fault

326 activity, consequently, C1, C2 and C3 cementation phases occurred prior to the proper fault
 327 plane and



328
 329 **Figure 7:** Paragenetic sequence of the both fault zones (black: Castellás, grey: D19) with micro-porosity development (blue),
 330 cementation (orange) and fault zone activation events (red).

331 fault core formation and are related to the fault nucleation. Replacive dolomite is found within
 332 FR1 matrix (Fig. 5E), therefore, it developed after FR1 formation. Finally, the C4 cement can
 333 be noticed within FR2 matrix indicating that C4 cementation event post-dated FR2 formation.
 334 The fault rock 2 (FR2) developed during strike-slip reactivation of the studied faults. The
 335 combined superposition, overlap, cross-cutting principles and isotopic signature of cements
 336 brought out the chronology between phases, and revealed the paragenetic sequence (Fig. 7).

337 The Urgonian carbonates in La Fare anticline underwent 3 major diagenetic events, which
 338 impacted the host rock and/or the fault zones. We discriminate among diagenetic events that
 339 occurred before and during faulting.

340 a. Pre fault diagenesis – microporosity development

341 During Upper Barremian, just after deposition, micro-bores organisms at the sediment-water
 342 interface enhanced the formation of micritic calcitic envelopes on bioclasts, ooids and peloids
 343 (Purser, 1980; Reid and Macintyre, 2000; Samankassou et al., 2005; Vincent et al., 2007). This
 344 micritisation in marine conditions is typical for Urgonian low-energy inner platform
 345 environment (Fournier et al., 2011; Masse, 1976). Subsequently, C0 cement formed around
 346 grains giving rise to a solid envelop inducing the preservation of the original grain shape during
 347 the later burial compaction (Step 0 on Fig. 8). However, the majority of isotopic values **does**
 348 not fit in the Barremian sea water calcite box which ranges **from -4.00‰ to -1.00‰** for $\delta^{18}\text{O}$
 349 and from +1.00‰ to +3.00‰ for $\delta^{13}\text{C}$ (Fouke et al., 1996; Godet et al., 2006). Only two data

350 points pertaining to micritised grains show isotopic values close the Barremian sea water
351 calcite. The isotopic depletion of other data indicates the slight impact of C0 cementation on
352 isotopic values.

353 The next sub-phase of cementation C1a partly fills intergranular porosity. This non luminescent
354 cement with isotopic values ranging from -6.8‰ to -3.9‰ for $\delta^{18}\text{O}$ and from -1.0‰ to +1.3‰
355 for $\delta^{13}\text{C}$ is characteristic of mixed fluids. Léonide et al. (2014) measured a calcite cement S1,
356 near La Fare anticline with similar luminescence and isotopic range values (mean: $\delta^{18}\text{O} =$
357 -5.49‰ ; $\delta^{13}\text{C} = +2.34\text{‰}$). These authors linked this cementation phase to a shallow burial
358 meteoric fluid circulation under equatorial climate during Durancian uplift. This diagenetic
359 event led to micrite re-crystallization, and to the development of microporosity (MF3). Since
360 La Fare carbonates were exhumed at that time (Léonide et al., 2014) the meteoric fluids led to
361 similar diagenetic modifications (Step 1 on Fig. 8):

- 362 (i) Micrite re-crystallization and microporosity MF3 setup by Ostwald ripening
363 processes (Fig. 9B1a; Ostwald, 1886; Volery et al., 2010).
- 364 (ii) Cementation of C1a, partly filling intergranular porosity (Fig. 9B1b)

365 The micrite re-crystallization strongly increased rock porosity due to enhanced microporosity
366 (Fig. 9B1a). Resulting from this event, Urgonian carbonates formed a type III reservoir *sensu*
367 Nelson (2001).

368 b. Fault-related diagenesis – alteration of reservoir properties

369

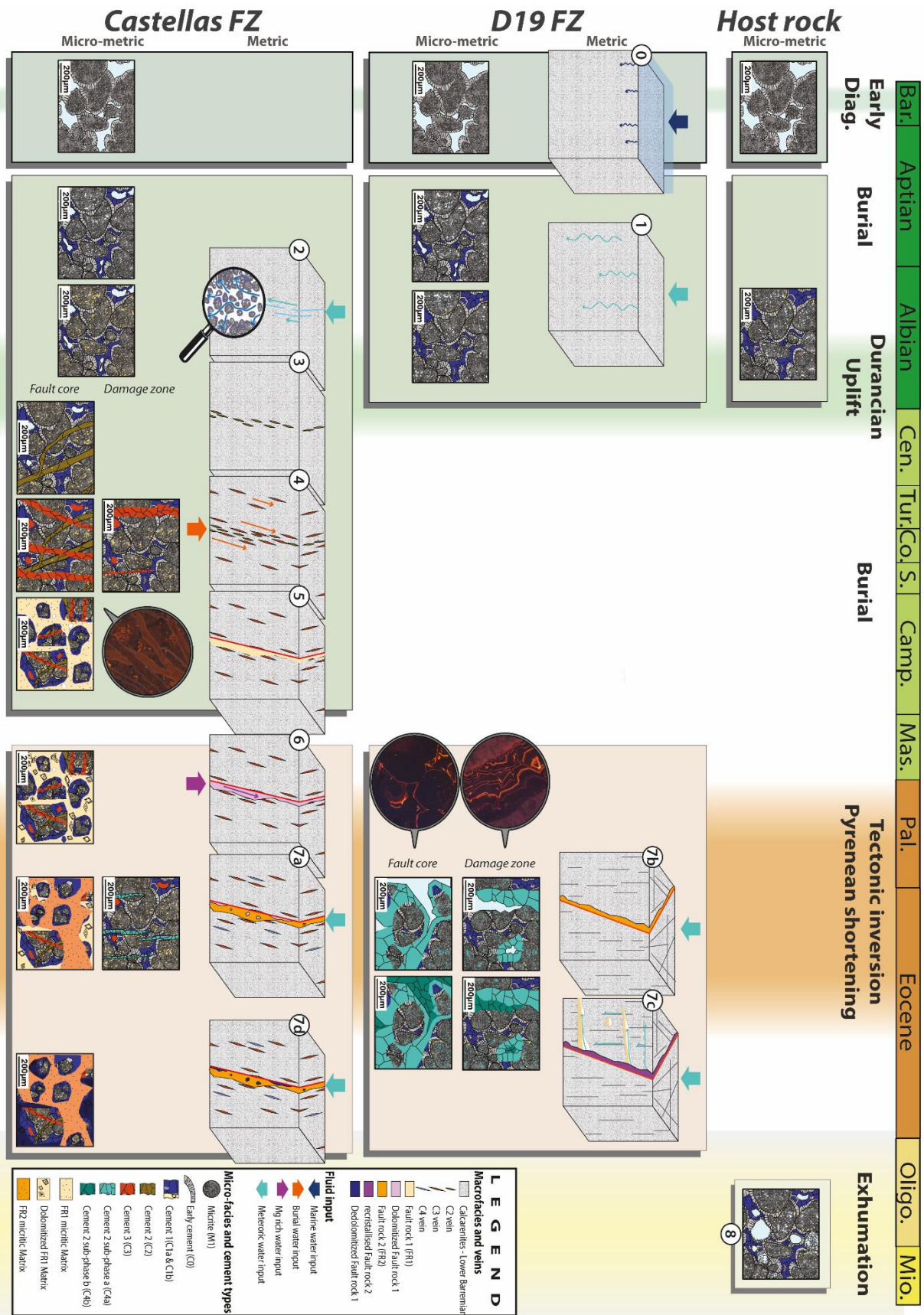
370 Normal faulting-related diagenesis

371 The Castellás fault first nucleated during Durancian uplift (Aubert et al., 2019b; Matonti et al.,
372 2012) affecting the host Urgonian carbonates.

373 In porous granular media, fault nucleation mechanisms can lead to dilation processes (Fossen
374 and Bale, 2007; Fossen and Rotevatn, 2016; Main et al., 2000; Wilkins et al., 2007; Zhu and
375 Wong, 1997) under low-confining pressure (<100 KPa; Alikarami and Torabi 2015). Because
376 this process leads to dilatancy, it increases the rock permeability (Alikarami and Torabi, 2015;
377 Bernard et al., 2002) in the first stage of deformation bands **development** (Heiland et al., 2001;
378 Lothe et al., 2002) enhancing fluid flows.

379 Castellás fault zone nucleated within a partially and dimly cemented host rock under low-
380 confining pressure, in an extensional stress regime, at a depth <1 km (Lamarche et al. 2012).
381 Under these conditions, Barremian host **rocks** were likely characterised by mechanical and
382 **petrophysical** properties close to porous granular media described above. Moreover, Micarelli
383 et al. (2006) showed that, during early stages of deformation, fault zones in carbonates have a
384 hydraulic behaviour comparable to deformation bands in carbonates. Hence, in the Urgonian
385 carbonates of La Fare area, dilatant processes occurred as an incipient fault mechanism and
386 enhanced fluid circulations along the deformation bands. Fluid flows led to the cementation of
387 C1b (Step 2 on Fig. 8). However, dilation bands were likely unstable and grain collapse occurred
388 swiftly after the beginning of the deformation due to an increase in the loading stress (Lothe et
389 al., 2002). **This could explain** why C1b does not fill all intergranular porosity. Consequently,
390 as all micritic grains in fault zone are cemented by C1b, the bulk isotopic measurements are
391 strongly influenced by C1 cement isotopic values. This is the explanation why in transect 3 the
392 bulk isotopic values 30 m apart from the fault (means of -5.26‰ for $\delta^{18}\text{O}$ and -0.82‰ for $\delta^{13}\text{C}$)

393 are close to bulk isotopic values far from the fault plane (188 m; -5.37‰ for $\delta^{18}\text{O}$ and -0.65‰
394 for $\delta^{13}\text{C}$, Fig. 6A). Dilation bands have also been described by *Kaminskaite et al.* (2019) in the
395 San Vito Lo Capo carbonates grainstones (Sicily, Italy). These dilation bands also led to
396 selective cementation of the carbonate rocks and to a microporosity decrease.

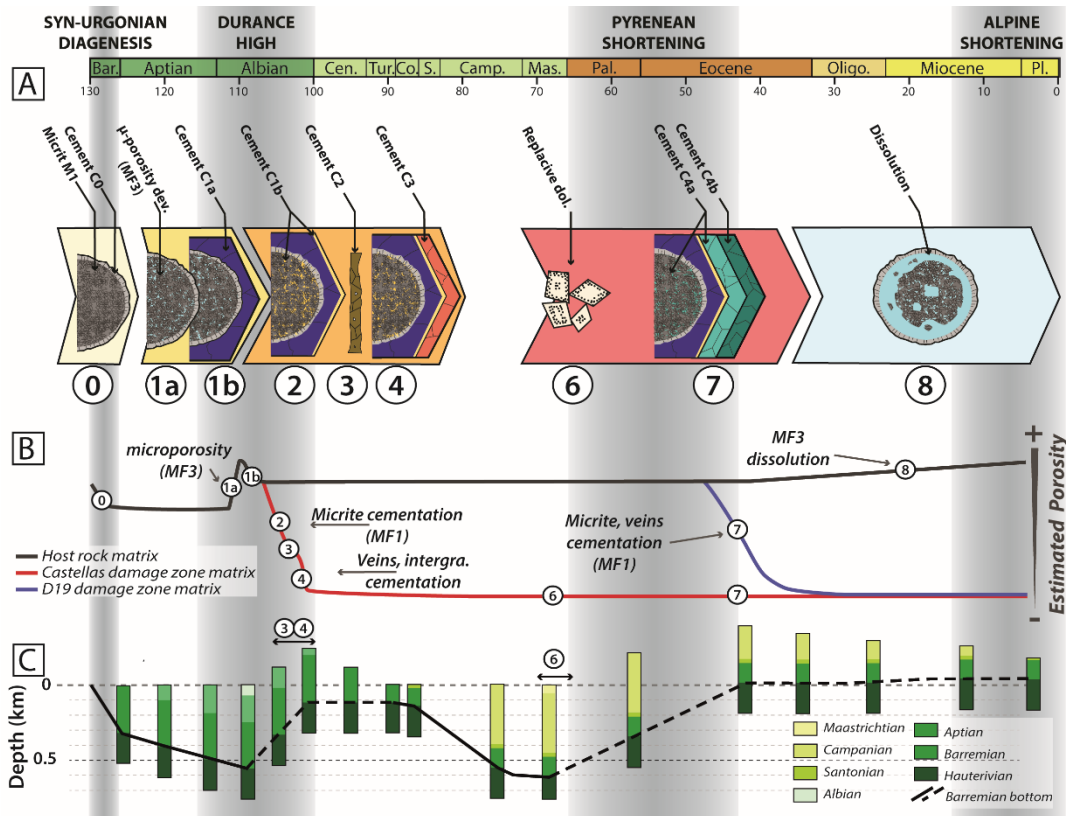


397

398

399

Figure 8 : Diagenetic and geodynamic evolution since the Barremian of both fault zones and host rock at the metric and micro-metric scale. Numbers 0 to 8 correspond to the steps 0 to 8 (see text for description).



401

402 **Figure 9** : Evolution of reservoir properties. A: different cementation phases; numbers 0 to 8 correspond to the steps 0 to
 403 8 (see text for description), B: relative porosity evolution of the host rock and the two fault zones; C: Burial/Uplift curve of
 404 Barremian basement (modified from Matonti et al. (2012)).

405 Cementation (C1a and C1b) conferred a stiffer response of limestone to deformation, making
 406 it prone to deform through brittle structures (joints and veins), rather than via granular
 407 particulate flow (deformation bands). During the first stages of fault evolution in low-porosity
 408 limestones, intense fracturing of the fault zone predating fault core formation is known to
 409 increase fault permeability (Micarelli et al., 2006). In the studied faults, the first brittle event
 410 allowed Al-rich fluids to flow with fine-grained quartz grains in the incipient open fractures
 411 leading to precipitation of C2 cement (Step 3 on Fig. 8). The Urgonian facies of the studied area
 412 are composed of pure carbonates without siliciclastic input. Quartz grains and Aluminium could
 413 have been reworked from surrounding formations. The rocks underlying the studied exposed
 414 Urgonian carbonates are limestones and dolostones. Albian and Aptian rocks are marly and
 415 sandy limestones, respectively (Anglada et al., 1977). Hence, Aptian layers are very likely to
 416 be the source of quartz. The fluids may have carried small grains of quartz from the Aptian
 417 sandy limestones via the fracture network. The Al enrichment of C2 could result from the
 418 erosion of Albian and Aptian deposits during the Durancian uplift (Guendon and Parron, 1985;
 419 Triat, 1982).

420 As the fault zone grew, new fracture sets formed, leading to new phase of calcite cementation
 421 (C3) in veins and intergranular porosity (Step 4 on Fig. 8). The $\delta^{18}\text{O}$ isotopic values of C3 range
 422 from -10.40‰ to -6.73‰ with $\delta^{13}\text{C}$ values between -2.09‰ and +1.22‰. As C3 cementation
 423 occurred during the Durancian uplift and denudation, it most probably did not cement in deep
 424 burial conditions (maximum depth of 500 m; Fig. 9C4). The negative $\delta^{13}\text{C}$ values tend
 425 corroborate the hypothesis of cementation induced by meteoric fluids rather than marine ones.
 426 Hence, C3 would correspond to a shallow burial/meteoric cementation phase. Due to this

427 cementation, rocks in this zone tightened with porosity down to <5%. The porosity did not
428 change since this event (Fig. 9B5). This porosity reduction due to cementation has also been
429 observed in other cases of brittle-dilatant faults (Agosta et al., 2007; Celico et al., 2006;
430 Gaviglio et al., 2009; Mozley and Goodwin, 1995). Following this, the fault zone was a barrier
431 to fluid flow, leading to a reservoir compartmentalization. Fluids responsible for precipitation
432 of C3 cement also occurred along fracture clusters of the D19 sector and led to vein formation.

433 In a later stage, the fault core formed and the fault plane *sensu-stricto* developed, leading to
434 FR1 breccia with a permeable matrix with quartz grains >100 µm in size (Step 5 on Fig. 8).
435 These grains either came from silica found inside C2 cement described above or from Aptian
436 overlying rocks. Silica crystals in C2 veins are scarce and smaller than 10 µm. Thus, quartz
437 grains may rather come from Aptian rocks like the ones found in C2 veins. The presence of
438 Aptian quartz in the fault core proves that the Castellás fault affected also Aptian rocks, which
439 were later eroded during the Durancian uplift. According to this, the fault activity occurred
440 before total erosion of Aptian rocks. Un-cemented breccias within the fault core formed good
441 fluid pathways (Billi et al., 2008; Delle Piane et al., 2016). In the studied fault, formation of
442 FR1 breccia allowed the fault core to act as a drain. However, the cemented surrounding host
443 rocks constrained the lateral extent of the drainage area of this high-permeable conduit. Un-
444 cemented breccias acting as good across- and along- fluid pathways were also described on
445 **Apennine** carbonate formations within fault cores of strike-**slip** and extensional faults (Billi et
446 al., 2003, 2008; Storti et al., 2003).

447 **Tectonic Inversion – Castellás fault-related dolomitization**

448 At the onset of the Pyrenean shortening, compressive stresses led to underground water
449 upwelling through the permeable fault core. This fluid flow triggered the dolomitization of FR1
450 matrix (Step 6 on Fig. 8). This matrix-selective dolomitization could have been favoured by
451 several factors:

- 452 (i) The matrix has higher permeability than cemented clasts with a smaller grain size,
453 hence a higher grain surface area (Machel, 2004);
- 454 (ii) This type of upwelling fluids, so-called “squeegee-type”, are **short-lived** processes
455 (Buschkuehle and Machel, 2002; Deming et al., 1990; Dorobek, 1989; Machel et
456 al., 2000) not favourable for massive dolomitization;
- 457 (iii) Low-temperature fluids, under 50°-80°C, enabled the preservation of FR1 clast
458 initial structure. Contrarily, high-temperature dolomitization tends to be destructive
459 (Machel, 2004);
- 460 (iv) The tight surrounding host rock constrained Mg-rich fluid circulation to the fault
461 core domain.

462 Gisquet et al. (2013) noticed similar **fault-related** replacive dolomitization phase in the Etoile
463 massif, 23 km South-Est of the studied zones. They linked the dolomitization to contractional
464 stress regime during the early (Late Cretaceous) Pyrenean shortening. According to these
465 authors, the tectonic stress led to low-temperature upwelling fluids likely Mg-enriched by the
466 dissolution of underlying Jurassic dolomites. The Jurassic dolomites also occur in La Fare
467 anticline. Since the fluids leading to dolomitization of fault core were low-temperature and
468 since dolomites occur underground, it is possible that the dolomitization in La Fare and in the
469 Etoile massif were similar and synchronous. Matrix dolomitization can increase inter-

470 crystalline and/or inter-particle porosity up to 13% but the later dolomite overgrowth reduces
471 the porosity and permeability (Lucia, 2004; Machel, 2004; Saller and Henderson, 2001). Hence,
472 in the first stages of dolomitization, the fault core was an important drain. After the growth of
473 dolomite crystals, the fault core turned into barrier (Fig. 9 B6 and C6)

474 **Sinistral tectonic inversion – meteoric alteration of reservoir properties**

475 The ongoing tectonic inversion with increasing compressive stresses eventually led to the
476 Castellás fault sinistral reactivation and to the onset of D19 fault zone (Aubert et al., 2019b).
477 Aubert et al. (2019a) has shown that this compression reactivated the pre-existing early N030°
478 background fractures (Step 7 on Fig. 8). This tectonic event formed FR2 in fault cores but with
479 specific diagenetic consequences. In the D19 fault zone, the fault nucleation and reactivation of
480 background fractures led to pluri-metric to kilometric fault surfaces with a permeable fault rock
481 acting as drains and localizing the fluid flow (Aubert et al., 2019a). This fluid flow witnessed
482 by the cementation of C4a and C4b in veins and micritised grains (MF1, Step 7c on Fig. 8), led
483 to a strong porosity decrease in the fault zone (Fig. 9, B7 and C7). However, not all fractures
484 were cemented by C4, so that fracture porosity/permeability was still partially preserved.
485 Therefore, the D19 fault zone became a type I reservoir *sensu* Nelson (2001) with a very low
486 matrix porosity/permeability and high fracture-related secondary permeability (Aubert et al.,
487 2019a).

488 Along F2, successive fluids gave rise to karsts, karstic infilling and dissolution/cementation
489 processes of FR2 matrix (Step 7c on Fig. 8). Then, FR2 was sealed by C4 cementation. Isotopic
490 values of C4 cement (from -9.2 to -6.1‰ for $\delta^{18}\text{O}$ and from -5.01‰ to -1.0‰ for $\delta^{13}\text{C}$) highlight
491 the strong influence of meteoric fluids. This is coherent with the occurrence of karstic infilling
492 due to fluid circulations in vadose zone, with alternating dissolution and cementation (Swart,
493 2015). However, the positive covariance between $\delta^{18}\text{O}$ and $\delta^{13}\text{C}$ of C4 suggests mixed fluids
494 (Allan and Matthews, 1982) of meteoric water and burial or marine water.

495 In the Castellás fault zone, the host rocks are slightly impacted by these meteoric fluid
496 circulations. Yet, some veins filled with C4a cement occur along transect 2 and 3 (Step 7a on
497 Fig. 8). Two samples have enriched $\delta^{18}\text{O}$ and $\delta^{13}\text{C}$ isotopic values (respective means of -6.25‰
498 and -4.20‰ for $\delta^{18}\text{O}$; -0.64 and -0.09‰ for $\delta^{13}\text{C}$) similar to C1 cement (Fig. 6A). This indicates
499 that C4 cement in the Castellás fault zone was precocious in comparison to the D19. C4 cement
500 in Castellás area is restricted to transect 2. Transect 2 cross-cuts the Castellás fault along a relay
501 zone (Fig. 2A). Relay or linkage zones occur where two fault segments overlap each other
502 during fault grow (Kim et al., 2004; Long and Imber, 2011; Walsh et al., 1999, 2003).
503 Consequently, the fault complexity, the fracture intensity and the fracture-strike range are
504 increased (Kim et al., 2004; Sibson, 1996). This process in the studied area resulted in a well-
505 connected fracture network that increased the permeability and favoured local fluid circulations.
506 In transect 2, the increase of the local permeability in the relay zone enhanced fluid flow related
507 to C4 cement. The relay zones along the Castellás fault and their consequences on the fracture
508 permeability are, therefore, responsible for this local cementation event. On the contrary,
509 cementation in D19 fault zone is linked to the highly permeable fault surfaces which acted as
510 drains (Aubert et al., 2019a). This implies that the cementation occurred only after the
511 development of the fault surface. In the case of Castellás, the relay zone was already present,
512 inherited from the former extensional activity, allowing early C4 fluid to flow through the fault
513 zone. This, in addition, explains why the early C4 cementation has not been recorded in D19

514 fault zone. The C4 cementation in transect 2 reduced porosity to less than 8% on a wider zone
515 (>60 m) than in both other transects (transect 1 ≈30 m, transect 3>40 m).

516 The reactivation of the Castellás fault formed a new fracture network that locally triggered the
517 fracture connectivity and permeability. The Castellás fault zone formed a type I reservoir
518 (Nelson, 2001), but lateral variation of the fracture network implies lateral variations of the
519 hydraulic properties. Thus, the fault zone was both a drain and a barrier (Matonti et al., 2012).
520 In this case, the most appropriate concept would be a sieve, because in this analogy, it is
521 synchronously closed in places and open in other places.

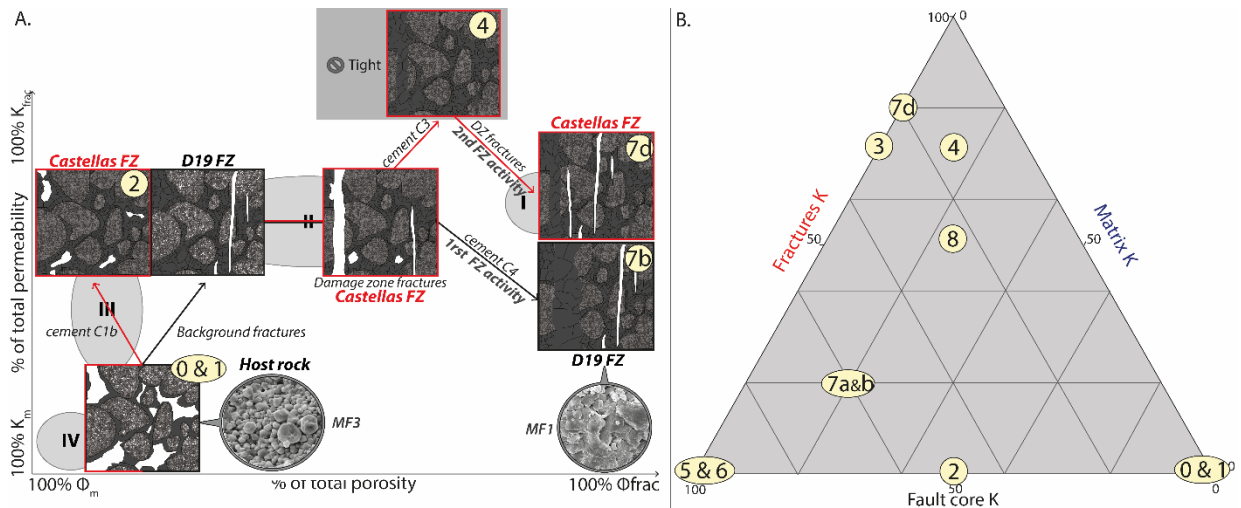
522 After these events, the matrix of the Castellás fault core was de-dolomitized (FR1) in relation
523 to cementation C5 (Step 7d on Fig. 8). The C5 cement isotope values (mean of -7.49‰ for $\delta^{18}\text{O}$
524 and -4.01‰ for $\delta^{13}\text{C}$) are comprised within C4 positive covariance between $\delta^{18}\text{O}$ and $\delta^{13}\text{C}$. This
525 indicates a continuity between C4 and C5 fluid flows. The measurements with the SEM
526 revealed a lack of Mg in the matrix indicating that C5 totally recrystallised the replacive
527 dolomite. Following this de-dolomitization phase, no additional diagenetic event is recorded in
528 Castellás fault zone.

529 A late Pyrenean to Alpine compression reactivated the D19 fault zone that formed the new fault
530 rock FR3. The matrix of this fault rock has very low $\delta^{13}\text{C}$ isotopic values (mean of -6.83‰)
531 indicating an organic matter input (Swart, 2015). This implies fluids percolating soils, as results
532 from a near surface fluid circulation. We deduce that the D19 faults was lately reactivated after
533 the folding of the La Fare anticline. There is no such cementation with similar isotope values
534 in the fault zone, meaning that fluids and cements did not alter the fault zone diagenetic
535 properties.

536 Eventually, the late exhumation of the Urganian carbonate host rocks led to flows inducing
537 dissolution of MF3 grains in the host rock. This phase produced the moldic porosity and
538 increased the porosity/permeability (Step 8 on Fig. 9B and C). These fluids, however, did not
539 affect fault zones.

540 2. EVOLUTION OF FAULT ZONES RESERVOIR PROPERTIES

541 The host rock presents a monophasic evolution and switch from a type IV reservoir where
542 matrix provided storage and flow, to a type III reservoir where fractures behave as pathways
543 towards fluid flow but the production mainly comes from the matrix (Nelson 2001, Fig. 10A).
544 The fault zones present a more complex polyphasic evolution than the host rock. Indeed, their
545 reservoir properties evolved from a type IV reservoir corresponding to the host rock to a type I
546 reservoir where fractures provide both storage and flow pathways (Nelson 2001, Fig. 10A).
547 Both fault zones present slight differences. The Castellás fault zone was completely tight soon
548 after C3 cementation. Consequently, it did not fit to the Nelson reservoir type classification.
549 However, after fault core formation, the fault zone presents a high fault core permeability. In
550 this study we propose a new approach with a triangle diagram taking into account fault core
551 permeability to remove the flaws of this method (Fig. 10B). The percentage assigned to the
552 fault core or to the matrix are qualitatively estimated. Further quantification could be evaluated,
553 for instance, with the width of the fault core and damage zone domains, or by estimating the
554 fracture network volume. However, no recent study have provided such quantification. Thus,
555 for Castellás fault zone, permeability evolves from a stage with exclusive contribution from the
556 host rock permeability (100% matrix; step 0 on Fig. 10B) to a permeability due to 50% to the



557

558 **Figure 10** : Castellias and D19 fault zone reservoir properties evolution. A: evolution of permeability and porosity taking into
 559 account fault zone fractures and matrix after Nelson (2001) and B: Triangle diagram of permeability evolution with 3
 560 components: matrix, fractures and fault core. Numbers 1 to 8 correspond to the steps 1 to 8 (see text for description). K:
 561 Permeability, Φ : Porosity, FZ: Fault Zone, DZ: Damage Zone, MF1 and MF3: Micrite micro-fabric.

562 matrix and 50% to the fault core during dilation band development (step 2 on Fig. 10B).
 563 Thereafter, during the two fracture events permeability is mainly linked to fracturing (C2: 30%
 564 fault core, 70% fractures; C3: 15% fault core, 15% matrix, 70% fractures; step 3, 4 on Fig.
 565 10B). Then, after fault core formation and during dolomitization event, permeability is solely
 566 provided by the fault core (step 6, 7 on Fig. 10B). Lastly, after fault zone reactivation, the
 567 permeability is due to 20% to the fault core and 80% to fractures (step 7c on Fig. 10B). The
 568 D19 fault zone permeability during its development was related for 20% to the matrix, 20% to
 569 the fractures and 60% to the fault core (step 7a and 7b on Fig. 10B).

570 8. CONCLUSION

571 This study deciphered the diagenetic evolution of two fault zones and the impact on reservoir
 572 properties of both faults and host rock in the frame of the overall geodynamic context of the SE
 573 Basin. The main outcomes are:

- 574 • Fault zones may have a complex diagenetic history, but most diagenetic phases occur
 575 during the nucleation of the fault. In the case of Castellias fault zone, the diagenetic
 576 imprint is mainly influenced by early diagenesis occurring along fractures and diffuse
 577 dilation zones prior to the proper fault plane nucleation. Regarding D19 fault zone, most
 578 of diagenetic alterations occurred just after fault onset in the first stage of its activity. In
 579 both cases, the cementation altered initial reservoir properties in the fault zone vicinity,
 580 switching from type III to type I during the first stages of fault development. Later fault
 581 reactivation slightly impacts matrix porosity/permeability.
- 582 • Fault zones act as drains canalizing fluid flows in the beginning of their development.
 583 This induces fault zone cementation but preservation of host rock microporosity. This
 584 important fluid drainage is visible on D19 outcrop where the flowing fluids led to
 585 dissolution/cementation of fault rock matrix and formed karsts.
- 586 • All diagenetic stages, including cementation and dolomitization, result from low-
 587 temperature fluids with important meteoric water input. These low-temperature fluid

588 flows associated with the deformation and cementation types, and, the lack of
589 mineralisation specific to high-temperature fluids disprove any significant hydrothermal
590 influence.

591 This regional study allows to draw broader rules for complex faults with polyphasic activity
592 affecting granular carbonates at shallow burial conditions (Fig. 9).

- 593 • Under extensional context, fault nucleation can lead to the development of dilation
594 bands acting as conduits for fluid flow. Carbonates are very sensitive to rock-fluids
595 interactions. Thus, the onset of dilation bands triggers important diagenetic reactions
596 that strongly alter local reservoir properties. During later fault zone development, the
597 diagenesis depends on fault zone internal architecture.
- 598 • Fracture networks related to fault nucleation in granular carbonates form good fluid
599 pathways before proper fault plane formation. However, in the case of pre-fractured
600 carbonates, like D19 fault zone, fault rocks early appear in fault cores. In these cases,
601 fluids flowed preferentially within the permeable breccia rather than in the damage
602 zone.

603

604 **Acknowledgement**

605 We would like to thank Suzan Verdegaal, Lionel Marié and Alain Tonetto for support they
606 provide during this study. We grateful to Editor Kei Ogata, and Fabrizio Agosta, Mattia Pizzati
607 and Eric Salomon who made critical suggestions to improve this paper.
608

609 REFERENCES

- 610 Agosta, F., Prasad, M. and Aydin, A.: Physical properties of carbonate fault rocks, Fucino Basin (Central Italy):
611 implications for fault seal in platform carbonates, *Geofluids*, 7, 19–32, doi:10.1111/j.1468-8123.2006.00158.x,
612 2007.
- 613 Agosta, F., Mulch, A., Chamberlain, P. and Aydin, A.: Geochemical traces of CO₂-rich fluid flow along normal
614 faults in central Italy, *Geophys. J. Int.*, 174(2), 1074–1096, doi:10.1111/j.1365-246X.2008.03792.x, 2008.
- 615 Agosta, F., Alessandrini, M., Antonellini, M., Tondi, E. and Giorgioni, M.: From fractures to flow: A field-based
616 quantitative analysis of an outcropping carbonate reservoir, *Tectonophysics*, 490(3–4), 197–213,
617 doi:10.1016/j.tecto.2010.05.005, 2010.
- 618 Agosta, F., Ruano, P., Rustichelli, A., Tondi, E., Galindo-Zaldívar, J. and Sanz de Galdeano, C.: Inner structure
619 and deformation mechanisms of normal faults in conglomerates and carbonate grainstones (Granada Basin, Betic
620 Cordillera, Spain): Inferences on fault permeability, *J. Struct. Geol.*, 45, 4–20, doi:10.1016/j.jsg.2012.04.003,
621 2012.
- 622 Alikarami, R. and Torabi, A.: Geomechanics for Energy and the Environment Micro-texture and petrophysical
623 properties of dilation and compaction shear bands in sand, *Geomech. Energy Environ.*, 3, 1–10,
624 doi:10.1016/j.gete.2015.06.001, 2015.
- 625 Allan, J. R. and Matthews, R. K.: Isotope signatures associated with early meteoric diagenesis, *Sedimentology*,
626 29(6), 797–817, doi:10.1111/j.1365-3091.1982.tb00085.x, 1982.
- 627 Allmendinger, R. W., Cardozo, N. and Fisher, D. M.: Structural geology algorithms: Vectors and tensors,
628 Cambridge Univ. Press, 9781107012, 1–289, doi:10.1017/CBO9780511920202, 2013.
- 629 Anglada, R., Arlhac, P., Catzigras, F., Colomb, E., Damiani, L., Durand, J. P., Durozoy, G., Guieu, G., Masse, J.
630 P., Nury, D., Philip, J., Rouire, J., Rousset, C., Roux, R. M. and Blanc, J. J.: Notice explicative. Carte géologique
631 de la France a 1/50 000. Martigues - Marseille., 1977.
- 632 Aubert, I., Lamarche, J. and Léonide, P.: Deciphering background fractures from damage fractures in fault zones
633 and their effect on reservoir properties in microporous carbonates (Urgonian limestones, SE France), *Pet. Geosci.*,
634 doi:DOI10.1144/petgeo2019-010, 2019a.
- 635 Aubert, I., Lamarche, J., Richard, P. and Leonide, P.: Imbricated Structure and Hydraulic Path Induced by Strike
636 Slip Reactivation of a Normal Fault in Carbonates, in Fifth International Conference on Fault and Top Seals, p. 4.,
637 2019b.
- 638 Bense, V. F., Gleeson, T., Loveless, S. E., Bour, O. and Scibek, J.: Fault zone hydrogeology, *Earth-Science Rev.*,
639 127, 171–192, doi:10.1016/j.earscirev.2013.09.008, 2013.
- 640 Bernard, X. Du, Eichhubl, P. and Aydin, A.: Dilation bands : A new form of localized failure in granular media,
641 29(24), 1–4, doi:10.1029/2002GL015966, 2002.
- 642 Besson, D.: Architecture du bassin rhodano-provençal miocène (Alpes , SE France) : relations entre déformation,
643 physiographie et sédimentation dans un bassin molassique d'avant-pays, Ecole des Mines, Paris., 2005.
- 644 Bestani, L.: Géométrie et cinématique de l'avant-pays provençal : Modélisation par coupes équilibrées dans une
645 zone à tectonique polyphasée, Aix-Marseille University, 2015.
- 646 Bestani, L., Espurt, N., Lamarche, J., Bellier, O. and Hollender, F.: Reconstruction of the Provence Chain
647 evolution, Southeastern France, *Tectonics*, 35, 1506–1525, doi:10.1002/2016TC004115, 2016.
- 648 Billi, A., Salvini, F. and Storti, F.: The damage zone-fault core transition in carbonate rocks: Implications for fault
649 growth, structure and permeability, *J. Struct. Geol.*, 25(11), 1779–1794, doi:10.1016/S0191-8141(03)00037-3,
650 2003.
- 651 Billi, A., Primavera, P., Soligo, M. and Tuccimei, P.: Minimal mass transfer across dolomitic granular fault cores,
652 *Geochemistry, Geophys. Geosystems*, 9(1), doi:10.1029/2007GC001752, 2008.
- 653 Borgomano, J., Masse, J., Maskiry, S. Al, Borgomano, J. and International, S.: The lower Aptian Shuaiba carbonate
654 outcrops in Jebel Akhdar, northern Oman: Impact on static modeling for Shuaiba petroleum reservoirs, *Bull. Am.
655 Assoc. Pet. Geol.*, 9(9), 1513–1529, doi:10.1306/61EEDCE2-173E-11D7-8645000102C1865D, 2002.
- 656 Borgomano, J., Masse, J. P., Fenerci-Masse, M. and Fournier, F.: Petrophysics of lower cretaceous platform
657 carbonate outcrops in provence (SE France): Implications for carbonate reservoir characterisation, *J. Pet. Geol.*,
658 36(1), 5–41, doi:10.1111/jpg.12540, 2013.
- 659 Bruna, P., Guglielmi, Y., Viseur, S., Lamarche, J. and Bildstein, O.: Coupling fracture facies with in-situ
660 permeability measurements to generate stochastic simulations of tight carbonate aquifer properties: Example from
661 the Lower Cretaceous aquifer , Northern Provence , SE France, *J. Hydrol.*, 529, 737–753,
662 doi:10.1016/j.jhydrol.2015.08.054, 2015.
- 663 Buschkuehle, B. E. and Machel, H. G.: Diagenesis and paleo fluid flow in the Devonian Southesk-Cairn carbonate
664 complex in Alberta, Canada, *Mar. Pet. Geol.*, 19, 219–227, doi:10.1016/S0264-8172(02)00014-4, 2002.
- 665 Caine, J. S., Evans, J. P. and Forster, C. B.: Fault zone architecture and permeability structure, *Geology*, 24(11),
666 1025–1028, doi:10.1130/0091-7613(1996)024<1025, 1996.
- 667 Cardozo, N. and Allmendinger, N. W.: Spherical projections with OSXStereonets, *Comput. Geosci.*, 51, 193–205,

668 doi:10.1016/j.cageo.2012.07.021, 2013.

669 Celico, F., Petrella, E. and Celico, P.: Hydrogeological behaviour of some fault zones in a carbonate aquifer of
670 Southern Italy: An experimentally based model, *Terra Nov.*, 18(5), 308–313, doi:10.1111/j.1365-
671 3121.2006.00694.x, 2006.

672 Champion, C., Choukroune, P. and Clauzon, G.: La déformation post-miocène en provence occidentale, *Geodin.*
673 *Acta*, 13(2–3), 67–85, doi:10.1080/09853111.2000.11105365, 2000.

674 Chester, F. M. and Logan, J. M.: Implications for Mechanical Properties of Brittle Faults from Observations of the
675 Punchbowl Fault Zone, California, *PAGEOPH*, 124(1/2), 79, doi:10.1007/BF00875720, 1986.

676 Chester, F. M. and Logan, J. M.: Composite planar fabric of gouge from the Punchbowl Fault, California, *J. Struct.*
677 *Geol.*, 9(5–6), doi:10.1016/0191-8141(87)90147-7, 1987.

678 Delle Piane, C., Giwelli, A., Clennell, M. Ben, Esteban, L., Nogueira Kiewiet, M. C. D., Kiewiet, L., Kager, S.
679 and Raimon, J.: Frictional and hydraulic behaviour of carbonate fault gouge during fault reactivation — An
680 experimental study, *Tectonophysics*, 690(PartA), 21–34, doi:10.1016/j.tecto.2016.07.011, 2016.

681 Deming, D., Nunn, A. and Evans, D. G.: Thermal Effects of Compaction-Driven Groundwater Flow, 95(89), 6669–
682 6683, doi:10.1029/JB095iB05p06669, 1990.

683 Demory, F. R., Conesa, G. I., Oudet, J. U., Mansouri, H. A. and Münch, P. H.: Magnetostratigraphy and
684 paleoenvironments in shallow-water carbonates : The Oligocene- Miocene sediments of the northern margin of the
685 Liguro- Provençal basin (West Marseille , southeastern France), *Bull. Soc. géol. Fr.*, 1, 37–55,
686 doi:10.2113/gssgfbull.182.1.37, 2011.

687 Deville de Periere, M., Durllet, C., Vennin, E., Lambert, L., Bourillot, R., Caline, B. and Poli, E.: Morphometry of
688 micrite particles in cretaceous microporous limestones of the middle east: Influence on reservoir properties, *Mar.*
689 *Pet. Geol.*, 28(9), 1727–1750, doi:10.1016/j.marpetgeo.2011.05.002, 2011.

690 Deville de Periere, M., Durllet, C., Vennin, E., Caline, B., Boichard, R. and Meyer, A.: Influence of a major
691 exposure surface on the development of microporous micritic limestones - Example of the Upper Mishrif
692 Formation (Cenomanian) of the Middle East, *Sediment. Geol.*, 353, 96–113, doi:10.1016/j.sedgeo.2017.03.005,
693 2017.

694 Dorobek, S.: migration of orogenic fluids through the Siluro-Devonian Helderberg Group during late Paleozoic
695 deformation: constraints on fluid sources and implications for thermal histories of sedimentary basins presence, ,
696 159, 25–45, doi:10.1016/0040-1951(89)90168-6, 1989.

697 Eltom, H. A., Gonzalez, L. A., Hasiotis, S. T., Rankey, E. C. and Cantrell, D. L.: Paleogeographic and paleo-
698 oceanographic influences on carbon isotope signatures: Implications for global and regional correlation, Middle-
699 Upper Jurassic of Saudi Arabia, *Sediment. Geol.*, 364, 89–102, doi:10.1016/j.sedgeo.2017.12.011, 2018.

700 Espurt, N., Hippolyte, J. C., Saillard, M. and Bellier, O.: Geometry and kinematic evolution of a long-living
701 foreland structure inferred from field data and cross section balancing, the Sainte-Victoire System, Provence,
702 France, *Tectonics*, 31(4), doi:10.1029/2011TC002988, 2012.

703 Evans, J. P., Forster, C. B. and Goddard, J. V.: Permeability of fault-related rocks, and implications for hydraulic
704 structure of fault zones, *J. Struct. Geol.*, 19(11), 1393–1404, doi:10.1016/S0191-8141(97)00057-6, 1997.

705 Ferraro, F., Agosta, F., Ukar, E., Grieco, D. S., Cavalcante, F., Belviso, C. and Prosser, G.: Structural diagenesis
706 of carbonate fault rocks exhumed from shallow crustal depths: An example from the central-southern Apennines,
707 Italy, *J. Struct. Geol.*, 122(February), 58–80, doi:10.1016/j.jsg.2019.02.008, 2019.

708 Florida, S., Maliva, R. G., Missimer, T. M., Clayton, E. A. and Dickson, J. A. D.: Diagenesis and porosity
709 preservation in Eocene microporous limestones , *Sediment. Geol.*, 217(1–4), 85–94,
710 doi:10.1016/j.sedgeo.2009.03.011, 2009.

711 Ford, M., Duchene, S., Gasquet, D. and Vanderhaeghe, O.: Two-phase orogenic convergence in the external and
712 internal SW Alps, *J. Geol. Soc. London.*, 163(5), 815–826, doi:10.1144/0016-76492005-034, 2006.

713 Fossen, H. and Bale, A.: Deformation bands and their influence on fluid flow, 12(12), 1685–1700,
714 doi:10.1306/07300706146, 2007.

715 Fossen, H. and Rotevatn, A. Fault linkage and relay structures in extensional settings — A review, *Earth Sci. Rev.*,
716 154, 14–28, doi:10.1016/j.earscirev.2015.11.014, 2016.

717 Fouke, B. W., Everts, A. W., Zwart, E. W. and Schlager, W.: Subaerial exposure unconformities on the Vercors
718 carbonate platform (SE France) and their sequence stratigraphic significance, *Geol. Soc. London, Spec. Publ.*, 104,
719 295–319, 1996.

720 Fournier, F. and Borgomano, J.: Critical porosity and elastic properties of microporous mixed carbonate-
721 siliciclastic rocks, *Geophysics*, 74(2), E93–E109, doi:10.1190/1.3043727, 2009.

722 Fournier, F., Leonide, P., Biscarrat, K., Gallois, A., Borgomano, J. and Foubert, A.: Elastic properties of
723 microporous cemented grainstones, *Geophysics*, 76(6), E211–E226, doi:10.1190/geo2011-0047.1, 2011.

724 Gattacceca, J., Deino, A., Rizzo, R., Jones, D. S., Henry, B., Beaudoin, B. and Vadeboin, F.: Miocene rotation of
725 Sardinia: New paleomagnetic and geochronological constraints and geodynamic implications, *Earth Planet. Sci.*
726 *Lett.*, 258(3–4), 359–377, doi:10.1016/j.epsl.2007.02.003, 2007.

727 Gaviglio, P., Bekri, S., Vandycke, S., Adler, P. M., Schroeder, C., Bergerat, F., Darquennes, A. and Coulon, M.:

728 Faulting and deformation in chalk, *J. Struct. Geol.*, 31(2), 194–207, doi:10.1016/j.jsg.2008.11.011, 2009.

729 Gisquet, F., Lamarche, J., Floquet, M., Borgomano, J., Masse, J. P. and Caline, B.: Three-dimensional structural
730 model of composite dolomite bodies in folded area (upper Jurassic of the Etoile massif, southeastern France), *Am.*
731 *Assoc. Pet. Geol. Bull.*, 97(9), 1477–1501, doi:10.1306/04021312016, 2013.

732 Godet, A., Bodin, S., Föllmi, K. B., Vermeulen, J., Gardin, S., Fiet, N., Adatte, T., Berner, Z., Stüben, D. and van
733 de Schootbrugge, B.: Evolution of the marine stable carbon-isotope record during the early Cretaceous: A focus
734 on the late Hauterivian and Barremian in the Tethyan realm, *Earth Planet. Sci. Lett.*, 242(3–4), 254–271,
735 doi:10.1016/j.epsl.2005.12.011, 2006.

736 Guendon, J.-L. and Parron, C.: Les phenomenes karstiques dans les processus de la bauxitisation sur substrat
737 carbonate. Exemple de gisement du sud est de la France, *Ann. la Société Géologique Belgique*, 108, 85–92, 1985.

738 Guieu, G.: Un exemple de tectonique tangentielle: l'évolution du cadre montagneux de Marseille, *Bull. la Société*
739 *Géologique Fr.*, 7 (T.IX N°, 610–630, 1967.

740 Guyonnet-Benaize, C., Lamarche, J., Masse, J. P., Villeneuve, M. and Viseur, S.: 3D structural modelling of small-
741 deformations in poly-phase faults pattern. Application to the Mid-Cretaceous Durance uplift, Provence (SE
742 France), *J. Geodyn.*, 50(2), 81–93, doi:10.1016/j.jog.2010.03.003, 2010.

743 Hammond, K. J. and Evans, J. P.: Geochemistry, mineralization, structure, and permeability of a normal- fault
744 zone, Casino mine, Alligator Ridge district, north central Nevada, 25, 717–736, doi:10.1016/S0191-
745 8141(02)00060-3, 2003.

746 Heiland, J., Raab, S. and Potsdam, G.: Experimental Investigation of the Influence of Differential Stress on
747 Permeability of a Lower Permian (Rotliegend) Sandstone Deformed in the Brittle Deformation, *Phys. Chem.*
748 *earth*, 26(1), 33–38, doi:10.1016/S1464-1895(01)00019-9, 2001.

749 Hodson, K. R., Crider, J. G. and Huntington, K. W.: Temperature and composition of carbonate cements record
750 early structural control on cementation in a nascent deformation band fault zone: Moab Fault, Utah, USA,
751 *Tectonophysics*, 690, 240–252, doi:10.1016/j.tecto.2016.04.032, 2016.

752 Hollis, C., Vahrenkamp, V., Tull, S., Mookerjee, A. and Taberner, C.: Pore system characterisation in
753 heterogeneous carbonates: An alternative approach to widely-used rock-typing methodologies, *Mar. Pet. Geol.*,
754 27(4), 772–793, doi:10.1016/j.marpetgeo.2009.12.002, 2010.

755 Kaminskaite, I., Fisher, Q. J. and Michie, E. A. H.: Microstructure and petrophysical properties of deformation
756 bands in high porosity carbonates, *J. Struct. Geol.*, 119(November 2018), 61–80, doi:10.1016/j.jsg.2018.12.001,
757 2019.

758 Kim, Y. S., Peacock, D. C. P. and Sanderson, D. J.: Fault damage zones, *J. Struct. Geol.*, 26(3), 503–517,
759 doi:10.1016/j.jsg.2003.08.002, 2004.

760 Knipe, R. J.: The influence of fault zone processes and diagenesis on fluid flow, *Diagenes. basin Dev. AAPG Stud.*
761 *Geol.*, 36, 135–154 [online] Available from:
762 <http://archives.datapubs.com/data/specpubs/resmi1/data/a067/a067/0001/0100/0135.htm>, 1993.

763 Knipe, R. J., Jones, G. and Fisher, Q. J.: Faulting, fault sealing and fluid flow in hydrocarbon reservoirs: an
764 introduction, *Geol. Soc. London, Spec. Publ.*, 147(1), NP LP-NP, doi:10.1144/GSL.SP.1998.147.01.21, 1998.

765 Lamarche, J., Lavenue, A. P. C., Gauthier, B. D. M., Guglielmi, Y. and Jayet, O.: Relationships between fracture
766 patterns, geodynamics and mechanical stratigraphy in Carbonates (South-East Basin, France), *Tectonophysics*,
767 581, 231–245, doi:10.1016/j.tecto.2012.06.042, 2012.

768 Lambert, L., Durllet, C., Loreau, J. P. and Marnier, G.: Burial dissolution of micrite in Middle East carbonate
769 reservoirs (Jurassic-Cretaceous): Keys for recognition and timing, *Mar. Pet. Geol.*, 23(1), 79–92,
770 doi:10.1016/j.marpetgeo.2005.04.003, 2006.

771 Laubach, S. E., Eichhubl, P., Hilgers, C. and Lander, R. H.: Structural diagenesis, *J. Struct. Geol.*, 32(12), 1866–
772 1872, doi:10.1016/j.jsg.2010.10.001, 2010.

773 Lavenue, A. P. C., Lamarche, J., Gallois, A. and Gauthier, B. D. M.: Tectonic versus diagenetic origin of fractures
774 in a naturally fractured carbonate reservoir analog [Nerthe anticline, Southeastern France, *Am. Assoc. Pet. Geol.*
775 *Bull.*, 97(12), 2207–2232, doi:10.1306/04041312225, 2013.

776 Leonide, P., Borgomano, J., Masse, J. and Doublet, S.: Relation between stratigraphic architecture and multi-scale
777 heterogeneities in carbonate platforms: The Barremian – lower Aptian of the Monts de Vaucluse, SE France,
778 *Sediment. Geol.*, 265–266, 87–109, doi:10.1016/j.sedgeo.2012.03.019, 2012.

779 Léonide, P., Fournier, F., Reijmer, J. J. G., Vonhof, H., Borgomano, J., Dijk, J., Rosenthal, M., Van Goethem, M.,
780 Cochard, J. and Meulenaars, K.: Diagenetic patterns and pore space distribution along a platform to outer-shelf
781 transect (Urgonian limestone, Barremian-Aptian, SE France), *Sediment. Geol.*, 306, 1–23,
782 doi:10.1016/j.sedgeo.2014.03.001, 2014.

783 Long, J. J. and Imber, J.: Geological controls on fault relay zone scaling, *J. Struct. Geol.*, 33(12), 1790–1800,
784 doi:10.1016/j.jsg.2011.09.011, 2011.

785 Lothe, A. E., Gabrielsen, R. H., Hagen, N. B. and Larsen, B. T.: An experimental study of the texture of
786 deformation bands: effects on the porosity and permeability of sandstones, (1990), doi:10.1144/petgeo.8.3.195,
787 2002.

788 Lucia, F. J.: Origin and petrophysics of dolostone pore space, *Geom. Petrog. Dolomite Hydrocarb. Reserv. Geol.*
789 *Soc. London, Spec. Publ.*, 235, 141–155, doi:10.1144/GSL.SP.2004.235.01.06, 2004.

790 Machel, H. G.: Concepts and models of dolomitization: a critical reappraisal, *Geol. Soc. London, Spec. Publ.*,
791 235(1), 7–63, doi:10.1144/GSL.SP.2004.235.01.02, 2004.

792 Machel, H. G., Cavell, P. A., Buschkuehle, B. E. and Michael, K.: Tectonically induced fluid flow in Devonian
793 carbonate aquifers of the Western Canada Sedimentary Basin, *Journal geochemical Explor.*, 70, 213–217,
794 doi:10.1016/S0375-6742(00)00093-5, 2000.

795 Main, I. G., Kwon, O., Ngwenya, B. T. and Elphick, S. G.: Fault sealing during deformation-band growth in porous
796 sandstone, *Geology*, 28(12), 1131–1134, doi:10.1130/0091-7613(2000)28<1131:FSDDGI>2.0.CO;2, 2000.

797 Masse, J.-P. and Philip, J.: Paléogéographie et tectonique du Crétacé moyen en Provence: révision du concept
798 d'isthme durancien., *Rev. Géographie Phys. Géologie Dyn.*, 18(1), 49–46, 1976.

799 Masse, J. P.: Les calcaires urgoniens de Provence (Valanginien-Aptien Inférieur) - Stratigraphie, paléontologie,
800 paléoenvironnements et leur évolution, Marseille, Thèse de la Faculté des Sciences de Luminy (U2), 1976.

801 Masse, J. P. and Fenerci-Masse, M.: Carbonate production by rudist bivalves. The record of Late Barremian
802 requieniid communities from Provence (SE France), *Palaeogeogr. Palaeoclimatol. Palaeoecol.*, 234(2–4), 239–
803 257, doi:10.1016/j.palaeo.2005.10.010, 2006.

804 Masse, J. P. and Fenerci Masse, M.: Drowning discontinuities and stratigraphic correlation in platform carbonates.
805 The late Barremian-early Aptian record of southeast France, *Cretac. Res.*, 32(6), 659–684,
806 doi:10.1016/j.cretres.2011.04.003, 2011.

807 Matonti, C., Lamarche, J., Guglielmi, Y. and Marié, L.: Structural and petrophysical characterization of mixed
808 conduit/seal fault zones in carbonates: Example from the Castellans fault (SE France), *J. Struct. Geol.*, 39, 103–
809 121, doi:10.1016/j.jsg.2012.03.003, 2012.

810 Micarelli, L., Benedicto, A. and Wibberley, C. A. J.: Structural evolution and permeability of normal fault zones
811 in highly porous carbonate rocks, *J. Struct. Geol.*, 28(7), 1214–1227, doi:10.1016/j.jsg.2006.03.036, 2006.

812 Molli, G., Cortecchi, G., Vaselli, L., Ottria, G., Cortopassi, A., Dinelli, E., Mussi, M. and Barbieri, M.: Fault zone
813 structure and fluid–rock interaction of a high angle normal fault in Carrara marble (NW Tuscany, Italy), *J. Struct.*
814 *Geol.*, 32(9), 1334–1348, doi:10.1016/j.jsg.2009.04.021, 2010.

815 Molliex, S., Bellier, O., Terrier, M., Lamarche, J., Martelet, G. and Espurt, N.: Tectonic and sedimentary
816 inheritance on the structural framework of Provence (SE France): Importance of the Salon-Cavaillon fault,
817 *Tectonophysics*, 501(1–4), 1–16, doi:10.1016/j.tecto.2010.09.008, 2011.

818 Moss, S. and Tucker, M. E.: Diagenesis of Barremian-Aptian platform carbonates (the Urganian Limestone
819 Formation of SE France): near-surface and shallow-burial diagenesis, *Sedimentology*, 42(6), 853–874,
820 doi:10.1111/j.1365-3091.1995.tb00414.x, 1995.

821 Mozley, P. S. and Goodwin, L. B.: Patterns of cementation along a Cenozoic normal fault: a record of paleoflow
822 orientations, *Geology*, 23(6), 539–542, doi:10.1130/0091-7613(1995)023<0539:POCAAC>2.3.CO;2, 1995.

823 Nelson, R.: *Geologic Analysis of Naturally Fractured Reservoirs*, second ed., 2001.

824 Ostwald, W.: *Lehrbuch der allgemeinen Chemie*, Verlag von Wilhelm Engelmann, Leipzig, 2, 909, 1886.

825 Philip, J.: Les formations calcaires à rudistes du Crétacé supérieur provençal et rhodanien, Thèse de Doctorat,
826 Université de Provence (Marseille), 1970.

827 Le Pichon, X., Bergerat, F. and Roulet, M.-J.: Plate kinematics and tectonics leading to the Alpine belt formation;
828 A new analysis, *Geol. Soc. Am.*, 218(March 1986), 111–131, doi:10.1130/SPE218-p111, 1988.

829 Pichon, X. Le, Rangin, C., Hamon, Y., Loget, N., Lin, J. Y., Andreani, L. and Flotte, N.: Geodynamics of the
830 France southeast basin, *Bull. la Soc. Geol. Fr.*, 181(6), 477–501, doi:10.2113/gssgfbull.181.6.477, 2010.

831 Purser, B. H.: Sédimentation et diagenèse des carbonates néritiques récents, *Les éléments de la sédimentation et*
832 *de la diagenèse*, Ed. Tech., 1, 366, 1980.

833 Reches, Z. and Dewers, T. A.: Gouge formation by dynamic pulverization during earthquake rupture, *Earth Planet.*
834 *Sci. Lett.*, 235(1–2), 361–374, doi:10.1016/j.epsl.2005.04.009, 2005.

835 Reid, R. P. and Macintyre, I. G.: Microboring Versus Recrystallization: Further Insight into the Micritization
836 Process, *J. Sediment. Res.*, 70(May), 24–28, doi:10.1306/2DC408FA-0E47-11D7-8643000102C1865D, 2000.

837 Roche, V.: Analyse structurale et géo-mécanique de réseau de failles du chaînon de La Fare les Oliviers (Provence),
838 *Univ. Montpellier 2*, 45, 2008.

839 Rossetti, F., Aldega, L., Tecce, F., Balsamo, F., Billi, A. and Brilli, M.: Fluid flow within the damage zone of the
840 Boccheggiano extensional fault (Larderello-Travale geothermal field, central Italy): Structures, alteration and
841 implications for hydrothermal mineralization in extensional settings, *Geol. Mag.*, 148(4), 558–579,
842 doi:10.1017/S001675681000097X, 2011.

843 Saller, A. H. and Henderson, N.: Distribution of Porosity and Permeability in Platform Dolomites: Insight from
844 the Permian of West Texas: reply, *Am. Assoc. Pet. Geol. Bull.*, 85, 530–532, doi:10.1306/090800850530, 2001.

845 Sallier, B.: Carbonates microporeux: influence de l'architecture du milieu poreux et de la mouillabilité sur les
846 écoulements diphasiques dans les réservoirs pétroliers, *Univ. Genève.*, 2005.

847 Samankassou, E., Tresch, J. and Strasser, A.: Origin of peloids in Early Cretaceous deposits, Dorset, South

848 England, Facies, 51(1–4), 264–273, doi:10.1007/s10347-005-0002-8, 2005.

849 Séranne, M.: The Gulf of Lion continental margin (NW Mediterranean) revisited by IBS: an overview, *Geol. Soc.*
850 *London, Spec. Publ.*, 156(1), 15–36, doi:10.1144/GSL.SP.1999.156.01.03, 1999.

851 Sibley, D. F. and Gregg, J. A. Y. M.: Classification of Dolomite Rock Texture, *J. Sediment. Petrol.*, 57(6), 967–
852 975, doi:10.1306/212F8CBA-2B24-11D7-8648000102C1865D, 1987.

853 Sibson, R. H.: Crustal stress, faulting and fluid flow, *Geol. Soc. London, Spec. Publ.*, 78(1), 69–84,
854 doi:10.1144/GSL.SP.1994.078.01.07, 1994.

855 Sibson, R. H.: Structural permeability of fluid-driven fault-fracture meshes, *J. Struct. Geol.*, 18(8), 1031–1042,
856 doi:10.1016/0191-8141(96)00032-6, 1996.

857 Sinisi, R., Petrullo, A. V., Agosta, F., Paternoster, M., Belviso, C. and Grassa, F.: Contrasting fault fluids along
858 high-angle faults: a case study from Southern Apennines (Italy), *Tectonophysics*, 690(PartA), 206–218,
859 doi:10.1016/j.tecto.2016.07.023, 2016.

860 Solum, J. G. and Huisman, B. A. H.: Toward the creation of models to predict static and dynamic fault-seal
861 potential in carbonates, *Pet. Geosci.*, 23(1), 70–91, doi:10.1144/petgeo2016-044, 2016.

862 Solum, J. G., Davatzes, N. C. and Lockner, D. A.: Fault-related clay authigenesis along the Moab Fault:
863 Implications for calculations of fault rock composition and mechanical and hydrologic fault zone properties, *J.*
864 *Struct. Geol.*, 32(12), 1899–1911, doi:10.1016/j.jsg.2010.07.009, 2010.

865 Storti, F., Billi, A. and Salvini, F.: Particle size distributions in natural carbonate fault rocks: Insights for non-self-
866 similar cataclasis, *Earth Planet. Sci. Lett.*, 206(1–2), 173–186, doi:10.1016/S0012-821X(02)01077-4, 2003.

867 Swart, P. K.: The geochemistry of carbonate diagenesis: The past, present and future, *Sedimentology*, 62(5), 1233–
868 1304, doi:10.1111/sed.12205, 2015.

869 Tempier, C.: Modèle nouveau de mise en place des structures provençales, *Bull. la Soc. Geol. Fr.*, 3, 533–540,
870 doi:10.2113/gssgfbull.III.3.533, 1987.

871 Tondi, E.: Nucleation, development and petrophysical properties of faults in carbonate grainstones: Evidence from
872 the San Vito Lo Capo peninsula (Sicily, Italy), *J. Struct. Geol.*, 29(4), 614–628, doi:10.1016/j.jsg.2006.11.006,
873 2007.

874 Triat, J.: Paléoaaltérations dans le crétacé supérieur de Provence rhodanienne, *Strasbourg: Institut de Géologie –*
875 *Université Louis-Pasteur.*, 1982.

876 Vincent, B., Emmanuel, L., Houel, P. and Loreau, J. P.: Geodynamic control on carbonate diagenesis: Petrographic
877 and isotopic investigation of the Upper Jurassic formations of the Paris Basin (France), *Sediment. Geol.*, 197(3–
878 4), 267–289, doi:10.1016/j.sedgeo.2006.10.008, 2007.

879 Volery, C., Davaud, E., Foubert, A. and Caline, B.: Shallow-marine microporous carbonatereservoir rocks in the
880 Middle East: relationship with seawater Mg/Ca ration and eustatic sea level, *J. Pet. Geol.*, 32(October), 313–325,
881 doi:10.1111/j.1747-5457.2009.00452.x, 2009.

882 Volery, C., Davaud, E., Foubert, A. and Caline, B.: Lacustrine microporous micrites of the Madrid Basin (Late
883 Miocene, Spain) as analogues for shallow-marine carbonates of the Mishrif reservoir formation (Cenomanian to
884 Early Turonian, Middle East), *Facies*, 56(3), 385–397, doi:10.1007/s10347-009-0210-8, 2010.

885 Walsh, J. J., Watterson, J., Bailey, W. R. and Childs, C.: Fault relays, bends and branch-lines, 21(8–9), 1019–
886 1026, doi:10.1016/S0191-8141(99)00026-7, 1999.

887 Walsh, J. J., Bailey, W. R., Childs, C., Nicol, A. and Bonson, C. G.: Formation of segmented normal faults: a 3-D
888 perspective, 25, 1251–1262, doi:10.1016/S0191-8141(02)00161-X, 2003.

889 Wilkins, S. J., Naruk, S. J., Wilkins, S. J., International, S., Naruk, S. J. and International, S.: Quantitative analysis
890 of slip-induced dilation with application to fault seal, 1(1), 97–113, doi:10.1306/08010605177, 2007.

891 Woodcock, N. H., Dickson, J. A. D. and Tarasewicz, J. P. T.: Transient permeability and reseal hardening in fault
892 zones: evidence from dilation breccia textures, *Geol. Soc. London, Spec. Publ.*, 270, 43–53, 2007.

893 Wu, G., Gao, L., Zhang, Y., Ning, C. and Xie, E.: Fracture attributes in reservoir-scale carbonate fault damage
894 zones and implications for damage zone width and growth in the deep subsurface, *J. Struct. Geol.*, 118(February
895 2017), 181–193, doi:10.1016/j.jsg.2018.10.008, 2019.

896 Zhang, Y., Schaub, P. M., Zhao, C., Ord, A., Hobbs, B. E. and Barnicoat, A. C.: Fault-related dilation,
897 permeability enhancement, fluid flow and mineral precipitation patterns: numerical models, *Geol. Soc. London,*
898 *Spec. Publ.*, 299(1), 239–255, doi:10.1144/SP299.15, 2008.

899 Zhu, W. and Wong, T.-F.: The transition from brittle faulting to cataclastic flow: Permeability evolution, *J.*
900 *Geophys. Res.*, 102(96), 3027–3041, doi:10.1029/96JB03282, 1997.

901

902